

**GENERATION OF FIBRONECTIN GRADIENTS
ON A PATTERNED SURFACE FOR NEURON GROWTH STUDIES**

by

Raphael J. Yoo

A thesis submitted to the Faculty of the University of Delaware in partial fulfillment of the requirements for the degree of Master of Science with a major in Chemistry and Biochemistry

Summer 2005

Copyright 2005 Raphael J. Yoo
All Rights Reserved

UMI Number: 1428259



UMI Microform 1428259

Copyright 2005 by ProQuest Information and Learning Company.
All rights reserved. This microform edition is protected against
unauthorized copying under Title 17, United States Code.

ProQuest Information and Learning Company
300 North Zeeb Road
P.O. Box 1346
Ann Arbor, MI 48106-1346

**GENERATION OF FIBRONECTIN GRADIENTS
ON A PATTERNED SURFACE FOR NEURON OUTGROWTH STUDIES**

by

Raphael J. Yoo

Approved: _____
Dr. Thomas P. Beebe, Jr., Ph.D.
Professor in charge of thesis on behalf of the Advisory Committee

Approved: _____
Dr. Charles G. Riordan, Ph.D.
Chair of the Department of Chemistry and Biochemistry

Approved: _____
Dr. Thomas Apple, Ph.D.
Dean of the College of Arts and Sciences

Approved: _____
Dr. Conrado M. Gempesaw II, Ph.D.
Vice Provost for Academic and International Programs

ACKNOWLEDGMENTS

I would like to thank my research advisor Dr. Beebe for his guidance and support throughout my graduate studies. I would also like to thank all the members of the Beebe Research Group for the memorable experiences together in the lab. I would like to give special acknowledgement to Zhanping Zhang, Matthew Wells, and Shawn Sullivan. Being senior members of the group, they showed unlimited patience and provided much helpful knowledge that I would have been lost without.

Another special thanks goes to Heather Egolf-Fox, who continued research on comb polymer height features, for which I was one of the main participants. A portion of this thesis is adapted from her work.

In addition, I'd like to thank Junqi Zheng of the Twiss Group at A.I. DuPont Children's Hospital. She provided her assistance in harvesting and preparing of the neurons for preliminary neuron growth on my gradient patterns.

I would also like to acknowledge the University of Delaware Department of Chemistry and Biochemistry for providing me with the opportunity to continue my education in the graduate program. Funding for this research was provided by the National Institutes of Health (NS43928 and EB000463).

TABLE OF CONTENTS

LIST OF TABLES	vi
LIST OF FIGURES	vii
ABSTRACT	ix
Chapter	
1 INTRODUCTION	10
1.1 Overview of the "Neuron Pathfinding Project"	10
1.2 Spinal Cord Injury (SCI) and Regeneration	11
1.3 Results and Discussion	14
1.3.1 GMBS Chemistry vs. F108-PDS Chemistry	14
1.3.2 Neuron Growth on Patterned Surfaces	17
1.4 Discussion/Future Studies	18
1.5 The Focus of My Research	20
2 SURFACE ANALYTICAL TECHNIQUES	22
2.1 Overview	22
2.2 Contact Angle	23
2.3 Atomic Force Microscopy	25
2.4 Time-of-Flight Secondary Ion Mass Spectrometry	28
2.5 X-ray Photoelectron Spectroscopy	33
2.6 Applications of Surface Sensitive Techniques	40
3 CONTROLLING NEURON GROWTH USING COMB POLYMER PATTERNED SUBSTRATES VIA MICRO-CONTACT PRINTING	41
3.1 Overview	41
3.2 Introduction	42
3.3 Experimental	45
3.3.1 Comb Polymer Synthesis and Characterization	45
3.3.2 Synthesis of PDMS Stamps	46

3.3.3	Patterning of Comb Polymer	47
3.3.4	AFM Imaging and Analysis of Patterned Surfaces	48
3.4	Results and Discussion	48
3.5	Conclusions and Suggested Future Studies	49
4	GENERATION OF GRADIENTS OF FIBRONECTIN ON PATTERNED SURFACES FOR NEURON GROWTH STUDIES	52
4.1	Overview	52
4.2	Introduction	52
4.3	Experimental	54
4.3.1	Surface Modification Using GMBS Crosslinker Chemistry	54
4.3.2	Generation of Fibronectin Gradients on Unpatterned Samples	55
4.3.3	Generation of Patterned Gradient Samples	58
4.3.4	Contact angle measurement	60
4.3.5	TOF-SIMS	60
4.3.6	XPS	61
4.3.7	Neuron plating	62
4.4	Results and Discussion	62
4.4.1	Contact Angle Measurements of the GMBS Crosslinker Chemistry	63
4.4.2	TOF-SIMS Characterization of Unpatterned and Patterned FN Gradients	63
4.4.3	XPS Characterization of Unpatterned and Patterned FN Gradients	66
4.4.4	Preliminary Neuron Growth Studies	67
4.5	Conclusion/Future Studies	67
	REFERENCES	73

LIST OF TABLES

4.1	Contact angle measurement comparison for each step of the GMBS Crosslinker Chemistry.....	63
-----	----------------------------------------------------------------------------------------------	----

LIST OF FIGURES

1.1	The anatomy of a neuron.....	11
1.2	Schematic diagram of GMBS and F108-PDS surface chemistries	15
1.3	Comparison of DRG growth on GMBS vs. F108-PDS surfaces	16
1.4	Neuron outgrowth on an FN/comb polymer patterned surface.....	17
2.1	Schematic diagram of a contact angle apparatus	23
2.2	Contact angle measurements of Piranha-clean, MTS, and GMBS- modified substrates.....	24
2.3	Schematic diagram of the AFM apparatus	27
2.4	Diagram of the “collision cascade” in the SIMS process	29
2.5	Schematic diagram of TOF-SIMS instrumentation	31
2.6	Diagram of the XPS and AES phenomena.....	34
2.7	Schematic diagram of the XPS instrumentation	36
2.8	XPS survey spectrum of a GMBS-modified surface.....	38
2.9	XPS high-resolution spectrum of the C1s region of a GMBS- modified surface	39
3.1	Schematic diagram of μ CP process.....	43
3.2	Amphiphilic comb polymer.....	44
3.3	AFM line profile analysis of a patterned substrate	49
3.4	Effect of transfer weight and comb polymer solution concentration on apparent feature height	50

4.1	Schematic diagram of a custom-built motorized linear-motion gradient device	56
4.2	Generation of continuous and step gradient profile surfaces	57
4.3	Orientation of the printed pattern relative to the immersion axis, resulting in vertical and horizontal gradients of fibronectin	59
4.4	Positive-ion TOF-SIMS survey spectrum for a GMBS + FN-modified gradient	64
4.5	TOF-SIMS imaging of FN gradient substrates after 15 minutes and 120 minutes of total incubation time	65
4.6	XPS survey spectra of FN gradients after 15 minutes and 120 minutes of total incubation time	68
4.7	XPS high-resolution spectra of the C1s region of FN gradients after 15 minutes and 120 minutes of total incubation time	69
4.8	FN surface coverage on unpatterned and patterned gradient samples as a function of incubation time	70
4.9	Brightfield image of neuron growth on a patterned FN gradient	71

ABSTRACT

Spinal cord injury (SCI) is a devastating and often permanent injury that affects hundreds of thousands of people worldwide. The irreversible effects of SCI are due to the central nervous system's (CNS) limited ability to repair itself. Currently, a major area of research involves the study of biomaterial bridging substrates as a way of promoting neuron growth and regeneration of damaged CNS pathways. Biomaterial bridging substrates attempt to promote regeneration by offering ligands known to promote neuron growth. In order to fully understand the interactions between neurons and these bridging substrates, more studies need to be done at a molecular level.

In this study, gradients of fibronectin, an extracellular matrix protein (ECM) known to promote neuron growth, were generated with a simple “dipping” technique, using a custom-made motorized linear-motion device. In addition to gradients of fibronectin, the surfaces were additionally patterned via micro-contact printing (μ CP) of an amphiphilic comb polymer known to resist protein adsorption. Patterned gradient surfaces are helpful in neuron growth studies, by controlling the neuron growth that occurs on the substrates, allowing more accurate measurement and quantification. In addition, preliminary studies on neuron growth were performed on these gradient samples.

Chapter 1

INTRODUCTION

1.1 Overview of the “Neuron Pathfinding Project”

Spinal cord injury (SCI) is a devastating injury that currently affects 250,000-400,000 individuals in the United States alone. Over 11,000 new cases of SCI are reported each year, with nearly 60% of the victims ranging from 30 years of age and younger.¹ The irreversible effects of SCI are a result of the central nervous system's inability to repair itself due to white matter and a build-up of glial scar tissue at the site of injury. Much effort has been concentrated in developing techniques to bypass lesions or promote regeneration of injured pathways. One such method under extensive investigation is that of biomaterial bridging substrates.

Currently, a major area of research in our group involves the characterization of biomaterial bridging substrates with high specificity to examine neuron outgrowth and pathfinding at the molecular level. These projects are collectively termed the “Neuron Pathfinding Project” and serve to examine 4 specific aims: 1) Create well-characterized 2D and 3D substrates patterned with chemoattractive and chemorepulsive regions to study neurite outgrowth, 2) Study axonal growth on these biomolecular substrates *in vitro*, 3) Study membrane adhesiveness and growth cone dynamics by using AFM force measurements at the molecular level, and 4) Development of a more biologically compatible biomaterial graft applying results obtained from Aims 1-3.

1.2 Spinal Cord Injury (SCI) and Regeneration

The neuron is the “building block” of the nervous system. Although there are several different types of neurons, all neurons have three main features in common: the cell body, axon, and dendrites (See Figure 1.1).

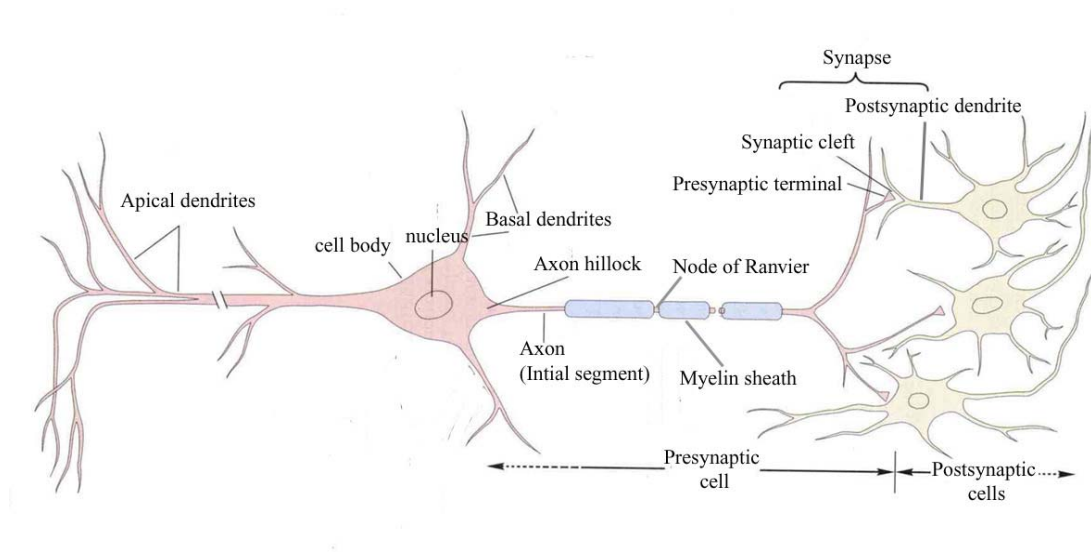


Figure 1.1 The anatomy of a neuron. (Modified and reprinted from Kandel, Schwartz, & Jessell, 1995)²

The neuron cell body contains the nucleus, which houses the genetic information that will determine neuron differentiation. From the cell body, two types of processes extend: the dendrites and the axon. Multiple dendrites branch out to receive information from other neurons by forming synaptic connections. Electrical signals known as action potentials are generated at the axon hillock of a neuron and propagated down the axon length to the presynaptic terminal. Many axons are insulated with a myelin sheath that is interrupted at regular intervals. These gaps are known as Nodes of Ranvier and help to increase the speed of transmission. This signal

is then transmitted onto the dendrites of a postsynaptic neuron. This signal can be transmitted in various forms, including another electric pulse or the release of neurotransmitters such as acetylcholine. In this manner, neurons create various signaling pathways and systems that are responsible for complex processes, such as sensation and movement.

The nervous system can be separated into two main components: the peripheral nervous system (PNS) and the central nervous system (CNS). The PNS consists of sensory and motor neurons running from stimulus receptors, muscles, and glands to the CNS. The CNS includes the brain, spinal cord, and the various neural pathways and connections between them. As mentioned previously, the CNS has very limited capability for regeneration after injury. As a result, damage occurring to the CNS, including spinal cord injuries (SCIs), often leads to irreversible and permanent conditions such as paralysis. However, regeneration in the PNS is markedly successful and often results in functional recovery of both motor and sensory functions.^{3,4} The inability of CNS neurons to regenerate does not appear to be inherent of the neurons, but rather is a result of the chemical environment the neurons experience at the site of CNS injury.

Classical studies have shown preliminary evidence that adult CNS neurons are capable of axonal elongation when presented with an environment mimicking that of the PNS.^{5,6} Since then, several groups have provided data supporting peripheral nerve grafts as well as grafts containing PNS olfactory ensheathing glial cells in their abilities to induce regeneration in adult CNS neurons.⁷⁻¹⁰ While CNS neurons show that they are capable of regeneration, it seems that the wound-healing environment of the CNS is ill suited for neuron growth. Recent studies

have identified several myelin-based proteins and factors as inhibitors of regeneration after injury to the CNS.¹¹⁻¹⁵

In addition to myelin-based factors and proteins, astrocytes play a major role in inhibition of CNS regeneration. Astrocytes are a subclass of glial cells that play a key role in axonal guidance and growth in the developing CNS.¹⁶⁻²⁴ During development, astrocytes express a variety of proteins that are found to promote neuronal attachment and outgrowth, among which include fibronectin (FN), laminin (LN), neural cell adhesion molecule (NCAM), and several other proteoglycans.²⁵⁻²⁹

Contrary to the role that astrocytes play during development, in the adult CNS they respond adversely to injury and are a major component of the scar tissue that prevents neuronal regeneration.^{28, 30-36} When injury to the CNS occurs, astrocytes in the vicinity of the lesion undergo a process known as “gliosis,” resulting in increased production of glial fibrillary acid protein (GFAP) and matrix proteins, which aggregate to produce what is known as a “glial scar.”^{6, 34, 35, 37} Some earlier studies have shown that regeneration is possible when glial scarring can be controlled and minimized.^{6, 34, 35, 37, 38} However, this is often not the case. Even in the presence of PNS grafts, the glial scar has been difficult to bypass.^{9, 39}

Currently, various studies are being conducted in hopes of designing therapeutic methods to overcome the inhibitory environment created at sites of injury in the CNS.^{7, 40-46} One area of high interest has been focused on the creation of biomaterial-bridging surfaces modified with extracellular matrix (ECM) proteins to overcome the glial scar. ECM proteins have been the main component used to modify biomaterial bridging substrates due to the extensive amount of literature that exists supporting their effects on neuronal outgrowth and growth cone pathfinding.⁴⁷⁻⁵² In

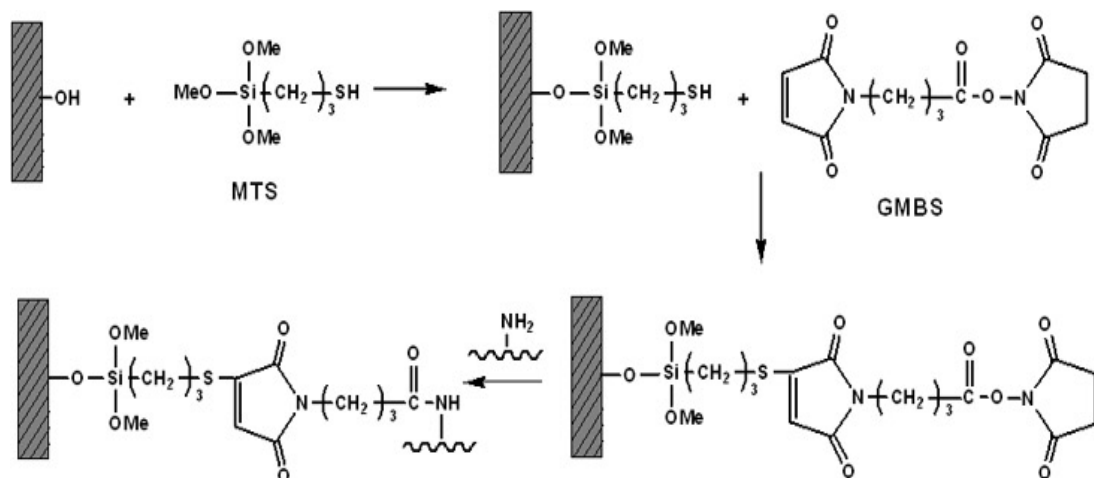
addition to whole proteins, substrates have also been modified with specific peptides and active sites of various ECM proteins.⁵²⁻⁵⁹

1.3 Results and Discussion

Our group's research on ECM and peptide modified substrates has yielded many promising results, including publications in various scientific journals (See references 52, 64, 65, 66, 86, 127, 129 and 130). Results from the past few years are reported in the following section.

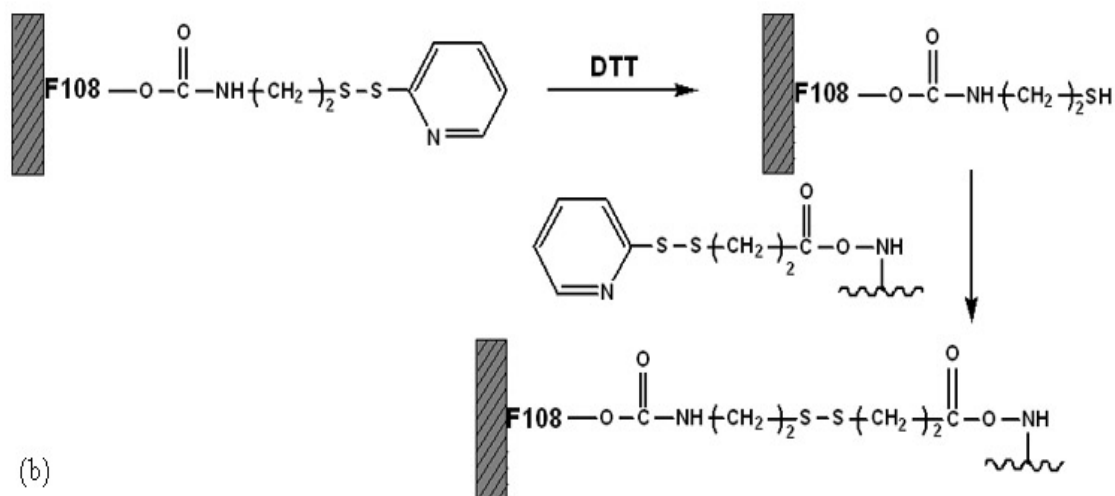
1.3.1 GMBS Chemistry vs. F108-PDS Chemistry

Surfaces and atomic force microscope (AFM) tips have been successfully modified to attach short peptides containing the RGD binding motif of FN as well as the whole protein itself. Surface modification was necessary to immobilize protein/peptides on the substrate rather than allow them to adsorb loosely to the surface. Substrates were modified using two different chemistries—the “Heterobifunctional Crosslinker” method⁶⁰ and the “PluronicsTM” method.⁶¹ The PluronicsTM method involves reduction of a pyridyl disulfide-activated F108 (F108-PDS) surface before peptide immobilization, while the Heterobifunctional Crosslinker method involves the covalent attachment of the crosslinker *N*- γ -maleimidobutyryloxy succinimide ester (GMBS) to provide a covalent linker for FN. The chemistries for both methods are detailed in Figure 1.2.



(a)

~~~~~ = protein or peptide



(b)

**Figure 1.2 Schematic diagrams for the a) Heterobifunctional Crosslinker method and the b) Pluronic<sup>TM</sup> method.** (Reprinted from Zhang et al. (2005) *Biomaterials*)

Each step of both surface chemistries, up to and including protein/peptide attachment, were analyzed and verified using various surface sensitive techniques, including: contact angle measurements, AFM, X-ray photoelectron spectroscopy (XPS), and time-of-flight secondary ion mass spectrometry (TOF-SIMS). A more detailed description of each of these techniques is presented in Chapter 2.

Both attachment chemistries were found to have good reproducibility, and were used in subsequent neuron growth studies. Results displayed in Figure 1.3 show neurons that were taken from postnatal 1-day-old rat dorsal root ganglia (DRG) experience far greater outgrowth on the protein/peptide-modified surfaces than on the corresponding control surface.

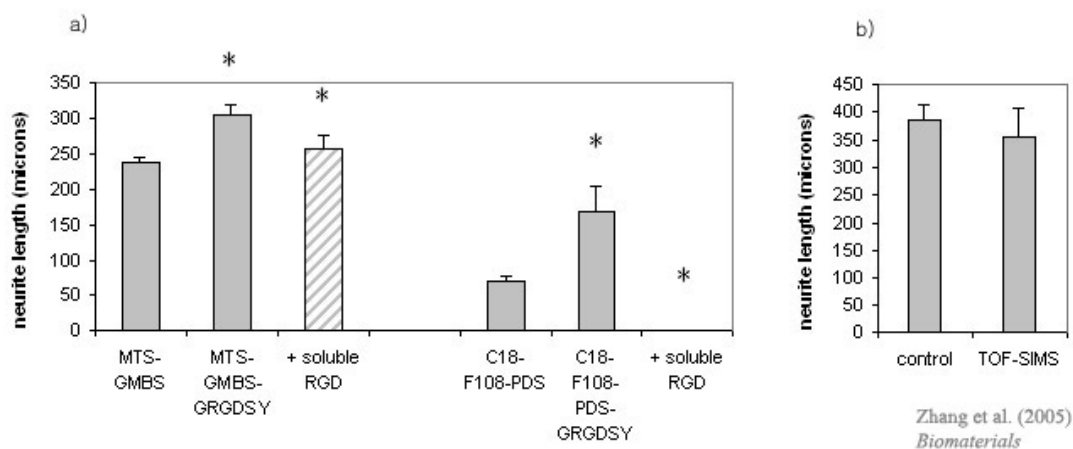


**Figure 1.3. Comparison of DRG neuron outgrowth after 24 hours incubation on: a) GMBS and F108-PDS chemistries, and b) a protein-modified GMBS control sample and a protein-modified GMBS sample that had been previously exposed to ultra-high vacuum conditions and analyzed by TOF-SIMS. (Reprinted from Zhang et al. (2005) *Biomaterials*)**

Additionally, the F108-PDS scheme was found to have reduced bioactivity compared to the GMBS scheme, which may be a result of the ratio of PDS activator to F108 polymer (1:50) compared to the amount of GMBS sites available for attachment.<sup>52</sup> Finally, there was no difference in neuron growth on a protein-modified GMBS control sample versus a sample that had been previously analyzed using TOF-SIMS and exposed to the ultra-high vacuum (UHV) environment. This indicates that the UHV environment of TOF-SIMS had no ill effects on the bioactivity of the GMBS to allow neuron attachment and growth, suggesting that neuron studies can be performed on actual analyzed substrates, rather than on unanalyzed parallel samples.

### **1.3.2 Neuron Growth on Patterned Surfaces**

In order to observe neurite outgrowth and attachment in a more controlled manner, substrates were further modified with a protein-resistive comb polymer patterned onto the surface via micro-contact printing ( $\mu$ CP).

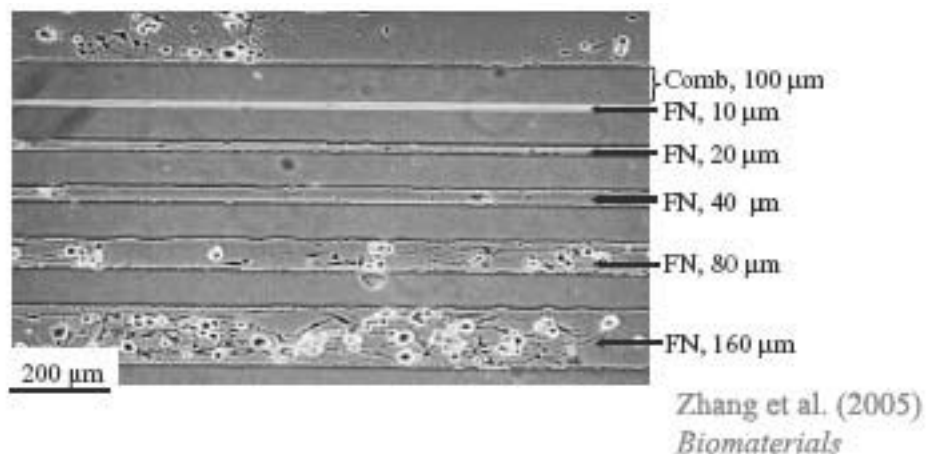


**Figure 1.4. Neuron outgrowth on an FN/comb polymer patterned surface.**  
(Reprinted from Zhang et al. (2005) *Biomaterials*)

Neurons were grown on substrates offering alternating chemattractive lanes of FN and chemorepulsive lanes of comb polymer of varying widths. (See Figure 1.4) Neurons were found to attach in the FN lanes as expected, but were also found to preferentially bind to FN lanes of larger width. A more detailed study on  $\mu$ CP and comb polymer feature effects on neuron growth will be presented in Chapter 3.

#### **1.4 Discussion/Future Studies**

Although the Neuron Pathfinding Project has yielded significant results, much still remains to be completed. Our research group has shifted its attention to substrate modification using only the GMBS chemistry rather than the F108-PDS scheme. Looking back at Figure 1.1, one sees that the F108-PDS chemistry involves additional modification of the peptide/protein before successful attachment can occur. As a result, this may alter or adversely affect the protein/peptide's bioactivity. Using the GMBS chemistry provides a two-fold advantage in that it provides a more robust covalent surface attachment and does not require alternation of the protein/peptide to attach it to the surface.

In addition to fibronectin, the ECM protein laminin (LN) has also been shown to effectively support and promote neuron growth.<sup>50, 53, 55-59, 62</sup> Studies of neuron growth on substrates patterned with alternating lanes of LN and comb polymer are currently underway by other group members, as are dual-patterned FN-LN surfaces for the first time.

In order to fully understand the interplay between matrix proteins and the neuron growth cones that result in the neuron pathfinding mechanism, it will be necessary to study their interactions at the molecular level. As mentioned at the beginning of this chapter, part of the Neuron Pathfinding Project is aimed at the study

of growth cone dynamics using the AFM to conduct force-pull measurements. Force-pull measurements can be used to study adhesive forces and interactions between the neuron growth cone and ligand molecules. AFM force-pull measurements are performed by bringing an AFM cantilever, modified with either FN or LN peptides or whole proteins using the chemistries described earlier, into conformal contact with the neuron growth cone. The AFM tip is then retracted gently until the pulling force overcomes the adhesion force between the tip and the growth cone, resulting in a “pull-off” event.

These “pull-off” events involve the rupturing of one to several bonds between the peptide or protein molecules on the AFM tip and the receptors of the neuron growth cone. A statistical method based on Poisson statistics has been developed and refined in our group to allow measurement of individual or single-molecule bond-rupture forces.<sup>63</sup> This statistical method has been further detailed and studied within our research group on biotin-avidin and biotin-streptavidin interactions as a model for biological receptor-ligand systems.<sup>64-66</sup> These studies are allowing us to examine the forces occurring between the neuron growth cones and underlying ligands at the molecular level.

Our group’s studies have begun on designing a three-dimensional biologically compatible substrate for use as a graft (i.e. one that is implantable at the site of injury). One type of substrate being investigated is that of electrospun<sup>67-77</sup> polystyrene (PS) fibers. Neuron cell bodies have been found to attach successfully to the fibers following the physisorption of FN. These woven fiber mats are our initial attempts at producing biologically active 3-D substrates that have the potential for *in vivo* studies. Future studies will be directed at electrospinning of collagen—a

relatively nonimmunogenic ECM component that has been also shown to promote neuron attachment.<sup>78</sup> Collagen's structural and biological properties make it ideal for designing of 3-D tissue scaffolding.<sup>74</sup> Once made, these scaffolds will undergo the same rigorous surface characterization as our protein- and peptide-modified substrates to ensure their bioactivity, chemical compatibility, and structural stability.

### **1.5 The Focus of My Research**

Although neuron growth was successfully contained within the FN lanes on the patterned substrates shown in Figure 1.3, it remains unclear whether the neurons were restricted due to the protein-resistive nature of the comb polymer or the “topographical barrier” the comb polymer creates. When analyzed using AFM, the comb polymer features on these previously patterned substrates were found to be ~600-700 nm in height. The average neuron growth cone is only ~260 nm in height, while the ends of extending neurites are ~385 nm in height.<sup>79</sup> In order to decouple the “chemical” and “topographical” roles that the comb polymer plays, a more controlled study of  $\mu$ CP and patterning of comb polymer was necessary, and results are discussed further in Chapter 3.

Another fundamental question about the interactions between neurons and underlying ligands is how neuron outgrowth is affected by ligand density. There are two theories that exist to offer explanation of what occurs. One such theory is that neuron growth will resemble fibroblast migration over substrates, in which the fibroblasts achieve maximal migration rates at *intermediate* ligand density and decrease with greater ligand concentration.<sup>80</sup> The reasoning behind this behavior is that as ligand density on the surface increases, it provides extra “traction” for the migrating cells. However, above an optimal surface concentration, additional

increases in ligand density are thought to make the surface “sticky”, resulting in the migrating cells’ inability to disengage from the surface. A second theory suggests a neuron is more adaptive to its environment and is based on preliminary neuron studies that showed axonal extension on LN substrates reached a maximum rate with ligand density and then seemed to plateau and maintain that rate, regardless of increases in LN concentration.<sup>81</sup> This second model indicates that a neuron can sense chemical changes in its environment, including surface ligand density. Thus, neurons may be able to sense when a surface is “too sticky” and downregulate their receptor expression to maintain the maximal extension rate.

## Chapter 2

### SURFACE ANALYTICAL TECHNIQUES

#### **2.1 Overview**

In order to study outgrowth of neurons on biomaterial surfaces, detailed surface characterization is required to evaluate the success of the desired modifications. Surface characterization includes the determination of structure, spatial distribution, composition, and orientation of the chemical species and biomolecules on the surface. The use of state-of-the-art surface analytical tools in the fields of cell-surface interactions and biomaterials development is relatively rare. For many years, the mainstream biomedical and neuroscience communities have employed a "take what you get" approach following simple dipping techniques. Such approaches downplay the significance of the surface itself (because of a lack of knowledge about its structure and composition) and focus almost entirely on cellular responses and behavior, both of which have been able to be studied by these communities.

The Beebe Research Group at the University of Delaware maintains one of the most state-of-the-art surface analysis facilities in the nation. The lab is equipped with both X-ray photoelectron spectroscopy (XPS) and time-of-flight secondary ion mass spectrometry (TOF-SIMS) in addition to several other surface-sensitive techniques, including contact angle and atomic force microscopy (AFM). This chapter discusses each of these surface-sensitive techniques in brief detail.

## 2.2 Contact Angle

In my research, multiple steps of surface modification are made to the substrates prior to protein/peptide attachment. Contact angle provides a quick initial measurement by which to evaluate each of the various surface chemistries following modification. In this thesis, contact angle measurement was used as a preliminary check after each step of surface modification using the GMBS chemistry protocol. Surface wettability<sup>82</sup>, also known as a surface's hydrophobicity, is one of the parameters indicative of the surface properties, and can be quickly determined using contact angle measurement.

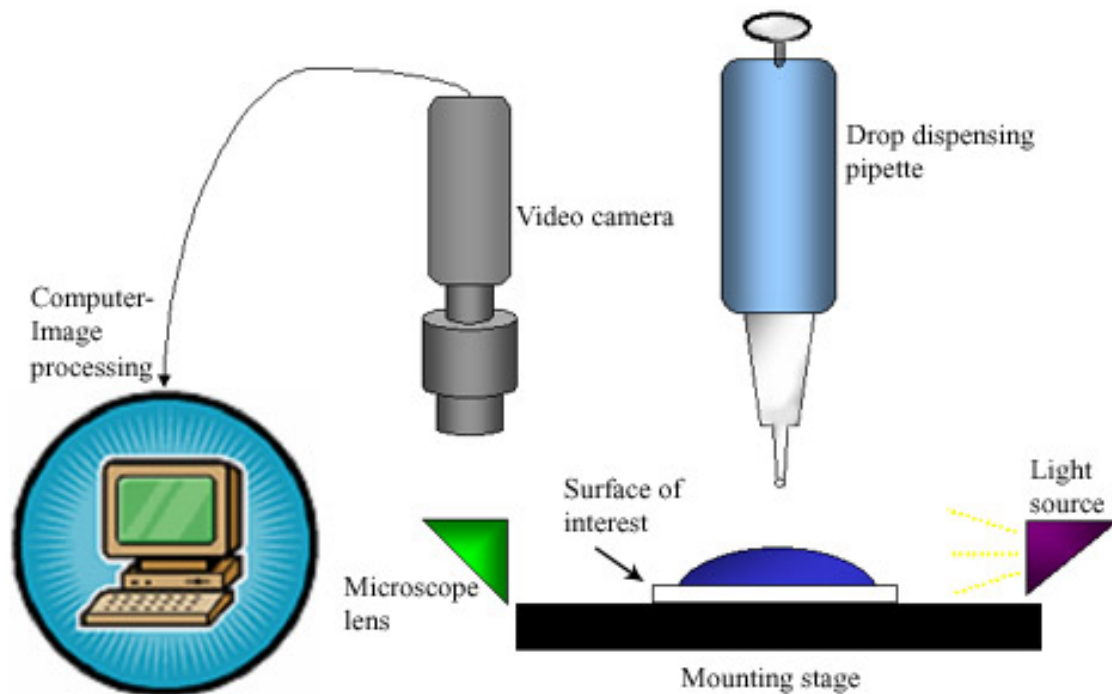


**Figure 2.1 Schematic diagram of a contact angle apparatus.**

The most common method used to obtain contact angle measurements is the sessile drop method. The sessile drop method involves use of an optical instrument called a goniometer, which is modified to take images of droplets placed on a surface of interest (See Figure 2.1). The contact angle,  $\theta$ , is referred to as the angle formed between the line tangent to the curve of the droplet and the baseline formed by the surface (See Figure 2.2).

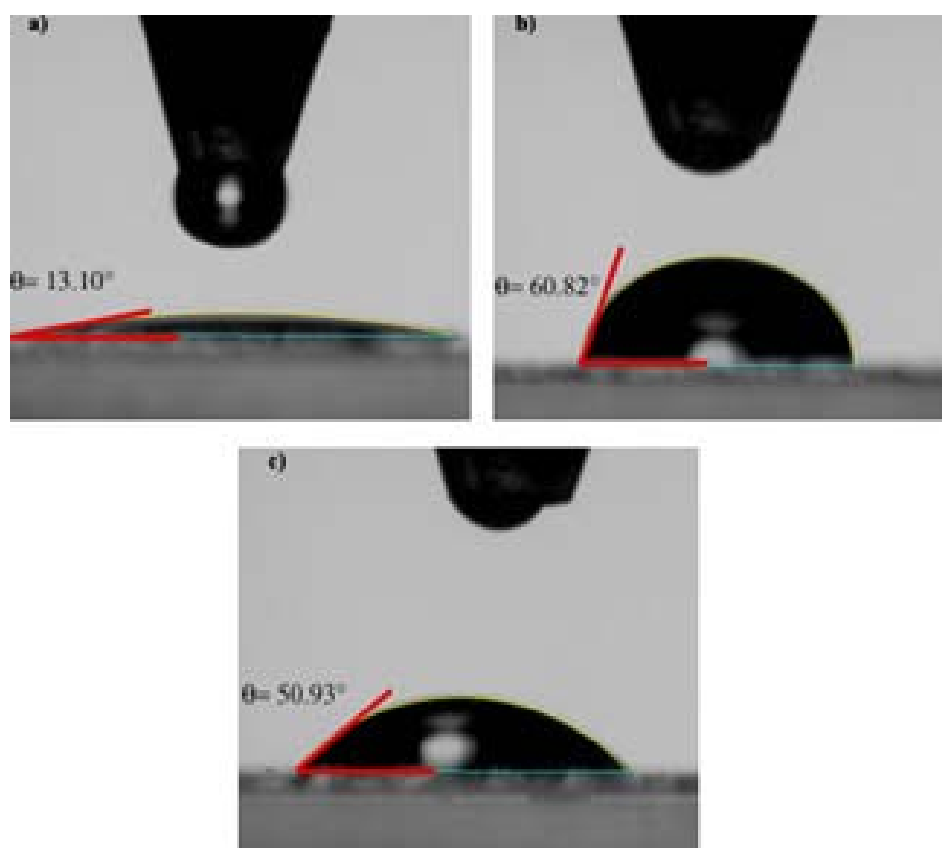


**Figure 2.2 Contact angle measurements of: a) a Piranha cleaned glass surface ( $13.10 \pm 1.2^\circ$ ), b) a glass surface modified with MTS ( $60.82 \pm 1.4^\circ$ ), and c) a glass surface modified with MTS and GMBS ( $50.93 \pm 1.6^\circ$ ).**

Typically, the droplet is dispensed from a syringe that is connected to a mounting stand holding the sample. A camera is used to capture images of the liquid droplet as it is lowered into contact with the surface and detaches from the tip of the syringe. The images are then processed by a computer equipped with software designed to calculate contact angle measurements.

Figure 2.2 provides an example of contact angle measurements taken from my research. FTA32 software v2.0 (First Ten Ångstroms, Portsmouth, VA) allows for video capture of the water droplet being applied to the surface. Using this software, the contact angle was measured from the first complete image of the water droplet right after it detached from the syringe. Sessile drops for contact angle measurement need not be limited to water, but can be a variety of pure liquid solvents or polymers depending on the surface being studied.

Contact angle measurement is not capable of highly specific surface characterization or quantification, and the information that it provides is averaged over the area of the liquid droplet (approximately 1 mm<sup>2</sup> to 0.2 mm<sup>2</sup>) However, it is still an effective tool in providing complementary data to that of more sophisticated techniques, to be discussed later in this chapter.

### **2.3 Atomic Force Microscopy**

Atomic Force Microscopy (AFM) is a scanning probe technique that generates a three-dimensional image of the surface with a spatial resolution that approaches atomic resolution. While the AFM can be used in many different ways, such as force-pull studies<sup>64-66</sup>, only the imaging mode of AFM will be discussed in the following section.

In AFM, the sample is mounted on a piezoelectric motor-driven stage. The ceramic crystals of the piezo expand or contract in direct proportion to an electric field, a phenomenon known as the *piezoelectric effect*. The piezoelectric motor takes advantage of the piezoelectric effect by converting applied electrical energy into mechanical energy (i.e. fine motor control). The piezoelectric motor-driven stage is capable of fine movements as small as just a few hundredths of nanometers to hundreds of microns. A cantilever with a sharp tip is brought down into contact with the surface and as it is rastered across an area in the  $x$ - and  $y$ - directions, a laser beam is aimed onto the back of the highly reflective cantilever. The cantilever bends in response to the topography of the surface, resulting in changes in deflection of the laser beam. The changes in the laser's deflection are measured by a photodiode detector and digitized to produce a three-dimensional image of the surface in various formats, such as height or phase contrast images. A schematic of the AFM apparatus and flow of information is presented in Figure 2.3.

AFM images can be obtained using three different modes—contact mode, non-contact mode, and intermittent contact mode. In contact mode, the cantilever tip maintains direct contact with the surface the entire duration of the scanning process. Contact mode is ideal for imaging of hard surfaces, as the surface morphology remains unaltered by the lateral forces produced during scanning. However, contact mode is often too “rough” for softer biological or polymer surfaces, and can cause damage to the surfaces being analyzed.

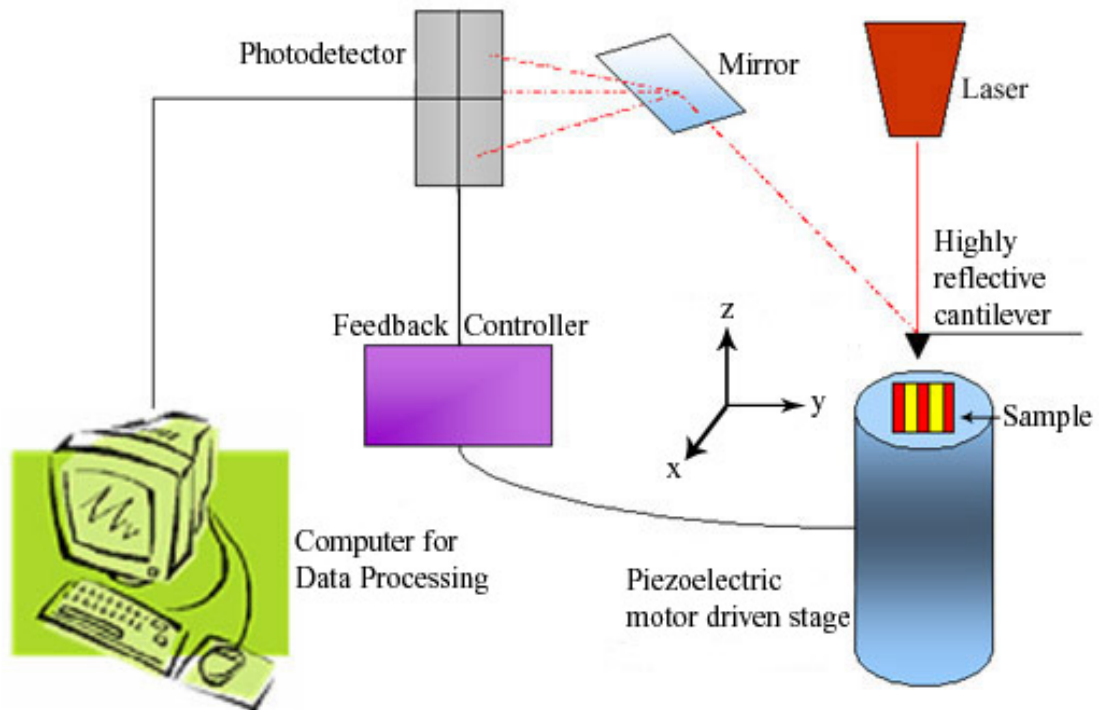


**Figure 2.3 Schematic diagram of the AFM apparatus.**

Non-contact mode works to minimize tip-sample interaction by allowing the tip to hover over the sample rather than make direct contact with the surface during scanning. Therefore, AFM images produced in non-contact mode are mainly the result of attractive forces between the tip and the surface. However, non-contact mode requires very fine tip-force control as well as a controlled environment with minimal contribution from external noise. Therefore, non-contact mode AFM is often operated in ultra-high vacuum (UHV) conditions. While it is capable of very high resolution, it also requires a significant amount of preparation time to fine-tune parameters and settings in addition to transferring of the sample in and out of UHV.

The third mode of AFM is intermittent contact mode, often referred to as “tapping mode.” The cantilever tip is oscillated at a defined frequency, causing the tip

to be periodically lifted off of the surface. Tapping mode provides the user with a compromise between the two other modes. Forces used in tapping mode are much softer than in contact mode, and since the tip maintains only intermittent contact with the surface, lateral forces are minimized. Additionally, tapping mode does not require the fine tip-force control and preparation time of non-contact mode. Therefore, tapping mode is ideal for studying softer biological/polymer substrates, as it provides high-resolution imaging in a short amount of time without causing damage to the surface.

#### **2.4 Time-of-flight Secondary Ion Mass Spectrometry (TOF-SIMS)**

The secondary ion mass spectrometry (SIMS) technique was initially developed and studied by Alfred Benninghoven in the 1970s<sup>83</sup>, and not until the 1980s was it combined with a highly efficient time-of-flight (TOF) analyzer to mark the birth of TOF-SIMS.<sup>84</sup> TOF-SIMS is a surface-sensitive technique that has gained immense popularity for its high surface sensitivity, detection limit, and its extensive application in the study of biological samples, including the large protein fibronectin.<sup>52, 85-89</sup> The following section provides a brief introduction about the principles governing the TOF-SIMS technique. A more detailed review of the technique is available in the literature.<sup>90-92</sup>

TOF-SIMS involves bombardment of a surface using a pulsed high-energy primary ion (for example  $\text{Ga}^+$  or  $\text{Cs}^+$  ions). Impact of these primary ions with the surface produces a collision cascade, leading to additional intramolecular collisions within the sample and mixing of layers, also known as “knock-on effects” (See Figure 2.4). These knock-on effects impart enough energy to molecules in the top 2-3 monolayers (ML) of the surface to overcome their binding energies and become

ejected from the sample. While the direct impact from the primary ion beam causes extensive fragmentation and leads to the ejection of single atoms and small molecule species, the knock-on effects cause little fragmentation, leading to the ejection of large molecular fragments.

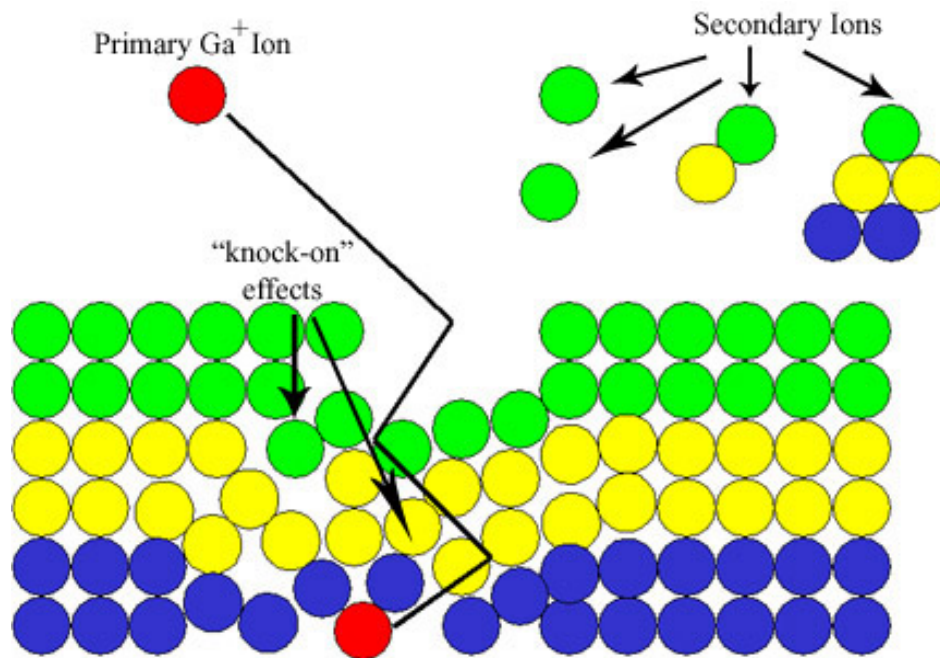


**Figure 2.4 Diagram of the collision cascade that occurs as a result of surface bombardment with a primary ion in TOF-SIMS.**

In TOF-SIMS, all of the secondary particles ejected by primary-ion bombardment enter into a field-free analyzer tube. Ions with identical kinetic energies, but differing masses will arrive at the detector at different times. The ion's flight time to the detector can be expressed in Equation 2.4.1, where  $t$  = flight time,  $m$  = mass of the ion,  $KE$  = kinetic energy, and  $D$  = length of the drift tube.

As indicated by Equation 2.4.1, lighter ions will reach the detector more quickly, while heavier ions will take longer to reach the detector.

$$t = (m/2KE)^{1/2} D \quad (2.4.1)$$

Secondary ions are separated according to their  $m/z$  (mass/charge) by the TOF analyzer, and the TOF-SIMS can be set to analyze either positive or negative ions. Secondary-ion intensities are plotted in a spectrum according to mass. In order to increase the signal/noise ratio, several spectra over the time course of an experiment are averaged or summed.

In order to increase the free-mean-path of the emitted particles in the TOF-SIMS process, a UHV environment is required so that secondary particles emitted from the surface do not experience any extraneous collisions with other particles in the atmosphere. An additional reason for UHV conditions is the need to maintain a contamination-free surface.

The first factor of high mass resolution ( $m/\Delta m$ ) is the time duration of the pulse width ( $\Delta t$ ) of the primary ion beam (ranging from a few tens of ps to a few tens of  $\mu$ s). It is important to note that to be able to achieve  $m/\Delta m$  equal to  $\sim 10,000$ ,  $\Delta t$  must be about 40 picoseconds. After bunching, the primary ion pulse width is a few tens of ps.

A second factor in the high mass resolution of the TOF-SIMS is its reflectron-based TOF analyzer (See Figure 2.5). During the emission process, energy and angular dispersion may occur, resulting in ions of identical mass with different initial velocities, which can lead to lower mass resolution.<sup>90</sup> The reflectron helps

compensate for energy and angular dispersion by exposing the secondary ions to a retarding electric field in the middle of the flight path.<sup>84</sup> This electric field allows ions of identical mass to “regroup” and depart the reflectron and arrive at the detector simultaneously, leading to higher sensitivity and mass resolution.

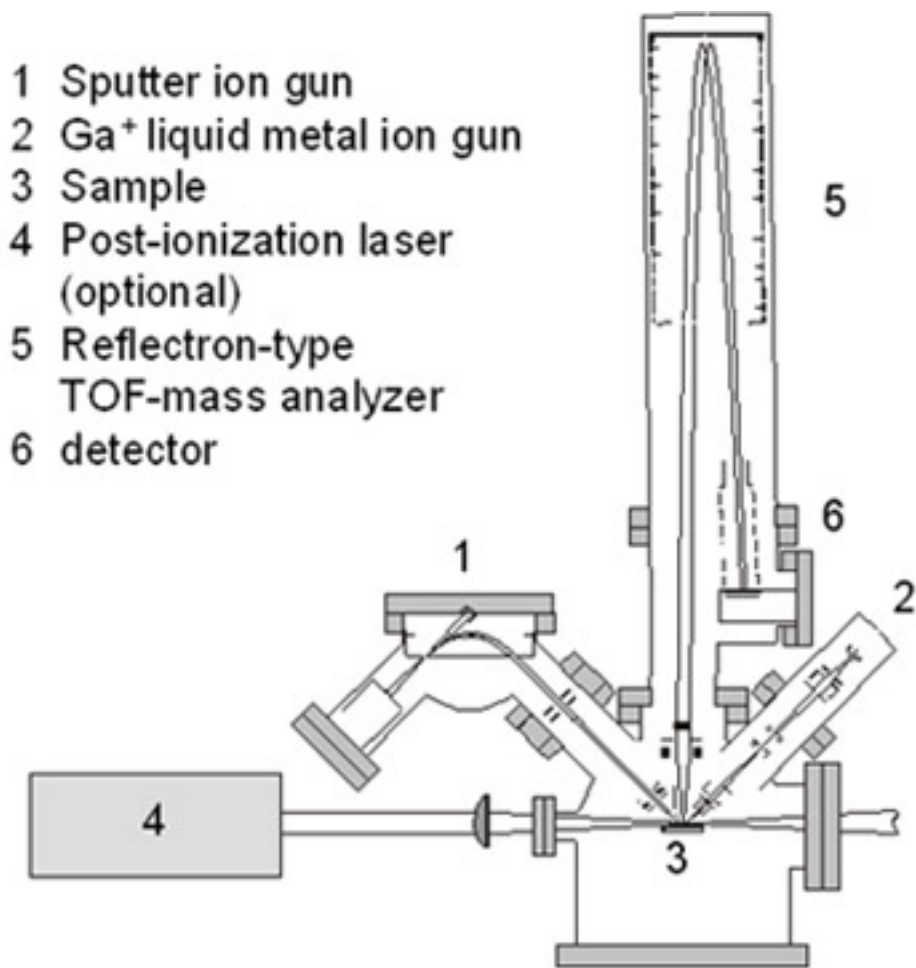


**Figure 2.5 A schematic diagram of the TOF-SIMS instrumentation.** (Schematic obtained from ION-TOF)

The TOF-SIMS can be run in two different modes: Static SIMS (spectra mode and imaging mode), and Dynamic SIMS. Static SIMS is typically used to obtain spectra to characterize and determine chemical structure/composition of the surface while causing “relatively” little sample damage. This is accomplished by setting a “static SIMS limit” to the pulsed ion beam dose. A monolayer of a surface typically has  $\sim 1 \times 10^{15}$  atoms/cm<sup>2</sup>. The pulsed Ga<sup>+</sup> ion beam used in static SIMS experiments uses less than  $\sim 10^{12}$  incident ions, or less than one in 1000 sites being damaged by a prior ion impact, thereby causing “negligible” damage to the surface. When the primary ion beam is further focused and rastered across a given area of the surface, lateral distribution of chemical information can be determined, effectively producing an image of the intensity of a particular mass as a function of (x, y) position on the surface.

Dynamic SIMS, more commonly known as “depth profiling,” is a much more destructive technique than Static SIMS. Depth profiling uses a secondary sputter beam (e.g. Cs<sup>+</sup> ion) to sputter away a certain layer of the surface, while simultaneously collecting spectra. In this manner, one can use depth profiling to analyze the depth distribution of chemical information, such as examining the presence of an oxide layer on a surface. Dynamic SIMS was not used in the present studies and will not be discussed further.

Though TOF-SIMS is a powerful surface analytical technique, it has a few drawbacks that make quantitative analysis very difficult. First, secondary ion yields are not directly proportional to that element’s concentration in the sample. Secondly, the TOF-SIMS sensitivity to a specific secondary ion will dramatically depend on that secondary ion’s ionization probability and *sputter yield*, which is the ratio of the

number of atoms sputtered to the number of impinging primary ions.<sup>90</sup> These are referred to as “matrix effects.” Matrix effects are the result of variability of secondary ion yield as the surface composition changes throughout the experiment.<sup>90</sup> Although multiple substrates may have the same modifications to their surfaces, secondary ion yields may not be exactly the same, making direct comparisons between samples difficult. The environment of a surface can change during analysis, leading to differential removal of species.<sup>90</sup> Also, the probability of ion formation may vary as a result of changes to the sample during the experiment.

Although TOF-SIMS provides information about the composition of the surface, only semi-quantitative information can be obtained. Therefore, TOF-SIMS is mainly used in conjunction with XPS to provide a more complete chemical profile of the structure with both qualitative and quantitative information.

## **2.5 X-ray Photoelectron Spectroscopy (XPS)**

X-ray photoelectron spectroscopy (XPS), also known as electron spectroscopy for chemical analysis (ESCA), is another surface-sensitive technique that is useful for determining the chemical and elemental composition of a sample’s surface. Although originally developed for studies of metal and semiconductor surfaces, recent research finds XPS being used more and more in the study of biological substrates, including those modified with laminin<sup>93-97</sup> and fibronectin.<sup>52, 85, 87, 89, 98, 99</sup> The following section provides a brief overview of the principles governing the XPS technique.

The technique of XPS is largely based on the *photoelectric effect*. In XPS, an x-ray photon penetrates deep into the sample, resulting in the excitation and ejection of core electrons from the surface (See Figure 2.6a).

$$E_k = E_{hv} - E_b - \phi_{sp} \quad (2.5.1)$$

The photoemission that occurs can be described by the equation 2.5.1 above, where  $E_k$  is the kinetic energy of the electron,  $E_{hv}$  is the x-ray photon energy,  $E_b$  is the binding energy of the electron, and  $\phi_{sp}$  is the workfunction of the spectrometer, a small instrumental correction.

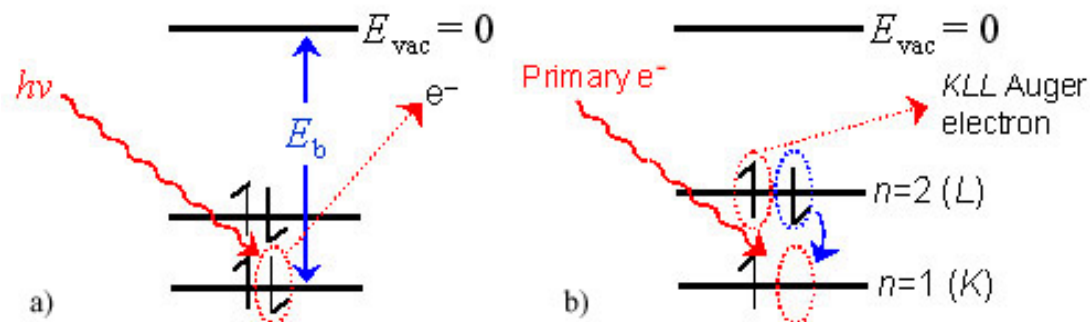


**Figure 2.6 Diagram of the a) XPS and b) AES processes.**

Typically, the XPS uses a monochromatic Al  $K\alpha$  or Mg  $K\alpha$  x-ray source with energy values of 1486.6 eV and 1253.6 eV, respectively. Core electrons are detected and an energy analyzer measures their kinetic energy. Since the  $E_{hv}$ ,  $E_k$ , and  $\phi_{sp}$  values are known or measurable, it is possible to calculate the binding energy of the core electrons ejected using Equation 2.5.1. The core electrons of every element, with the exceptions of hydrogen and helium, have unique binding energies that can be used to identify the different elements, giving valuable information about the chemical composition of the surface being studied.<sup>100</sup>

In addition to core electrons, a secondary process called the Auger process occurs, resulting in the ejection of additional electrons. The Auger process is a result of the electron hole left when the core electron is ejected by x-ray or electron beam irradiation (See Figure 2.6b). An electron from a higher-level shell moves to fill in the hole left by the core electron. Energy release is required for this process to occur, resulting in the emission of a third electron, which is the signal detected in Auger Electron Spectroscopy (AES). Although the technique will not be discussed, our XPS is capable of performing AES experiments. A more detailed review of AES can be found in the literature.<sup>101-103</sup>

XPS is considered a surface-sensitive technique because it examines the top 3-5 nm of a surface. The surface sensitivity of XPS is due to the inelastic mean-free path of electrons (IMFP). Electrons undergo inelastic scattering while traveling through the sample, resulting in a loss of energy. Only those electrons without significant energy loss from inelastic scattering will be detected, thus limiting the depth from which the detected photoelectrons can emerge. XPS is run under UHV conditions in order to eliminate extraneous gas phase collisions that could prevent electrons from reaching the detector. The photoelectrons are focused by several lenses and funneled through a hemispherical energy analyzer onto a channeltron or channelplate detector. A schematic diagram of an XPS instrument is presented in Figure 2.7.

XPS has several different modes aside from its standard application. XPS is capable of imaging the lateral distribution of species and producing intensity images acquired at different binding energies. XPS is also capable of depth profiling, while employing either a  $C_{60}$  or Ar gun to sputter the surface. Additionally, XPS is also

capable of angle-resolved XPS (ARXPS). ARXPS is accomplished by collecting electrons ejected at different emission angles to the surface plane, altering the surface sensitivity achieved. Additional information on ARXPS can be found in the literature.<sup>104, 105</sup> However, the remainder of this section will focus on standard applications of XPS in chemical identification and quantification.

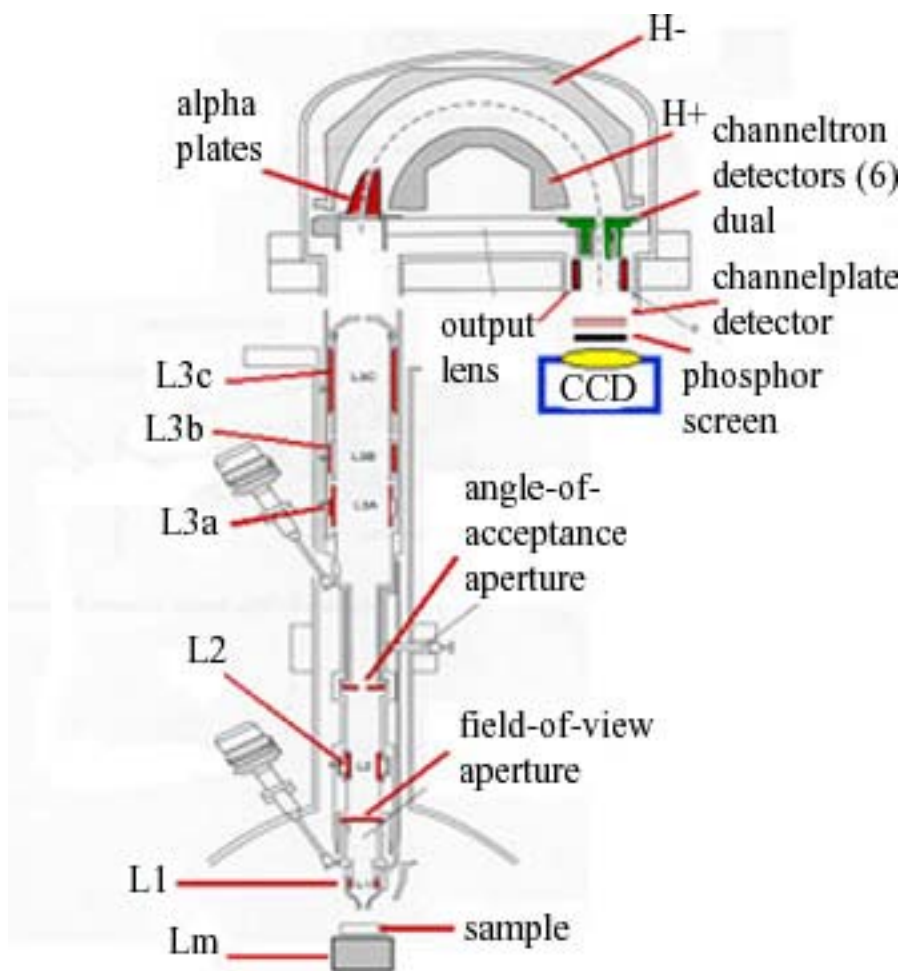


**Figure 2.7 Schematic diagram of the XPS instrumentation. The various parts labeled Lx represent focusing lenses, except for Lm, which represents the magnet.**

As mentioned, another important advantage of XPS is its capability of providing valuable quantitative information about the chemical composition of the surface. Seen in Figure 2.8 is an XPS survey spectrum of a GMBS-modified surface covalently linked with fibronectin. The survey spectrum examines a broad range of binding energies to provide a complete elemental profile of the surface.

In addition to the binding energies being unique for different elements, these binding energies are also sensitive to the chemical environment, or chemical state, of the atom.<sup>106</sup> This results in the ability to determine the chemical state in which an element is present on the surface, as well as resolving between different states. An example of chemical state identification can be seen in the following high-resolution XPS spectrum highlighting the C1s region of a GMBS-modified surface covalently linked with FN seen in Figure 2.9.<sup>52</sup> The spectrum shows that the binding energy curve can be fit with four different component peaks. After careful assignment based on the surface chemistry, carbon present on the surface can be identified in at least four different chemical states (-CH<sub>2</sub>-, -CH<sub>2</sub>N-, -CH<sub>2</sub>S-, -CH<sub>2</sub>O-, O=C-N, O=C-O).

In addition to qualitative identification of elements on the surface, XPS can provide quantitative information about the concentration of these elements. The equation for determining the atomic concentration of a given element or chemical species is given in Equation 2.5.2.<sup>100</sup> The atomic concentration,  $C_i$ , is determined by taking the intensity of the peak of interest,  $I_i$ , divided by its sensitivity factor,  $S_i$ , and dividing the resulting value by the sum of the ratios of all species on the surface divided by their respective sensitivity factors.

$$C_i = \frac{I_i / S_i}{\sum_i I_i / S_i} \quad (2.5.2)$$

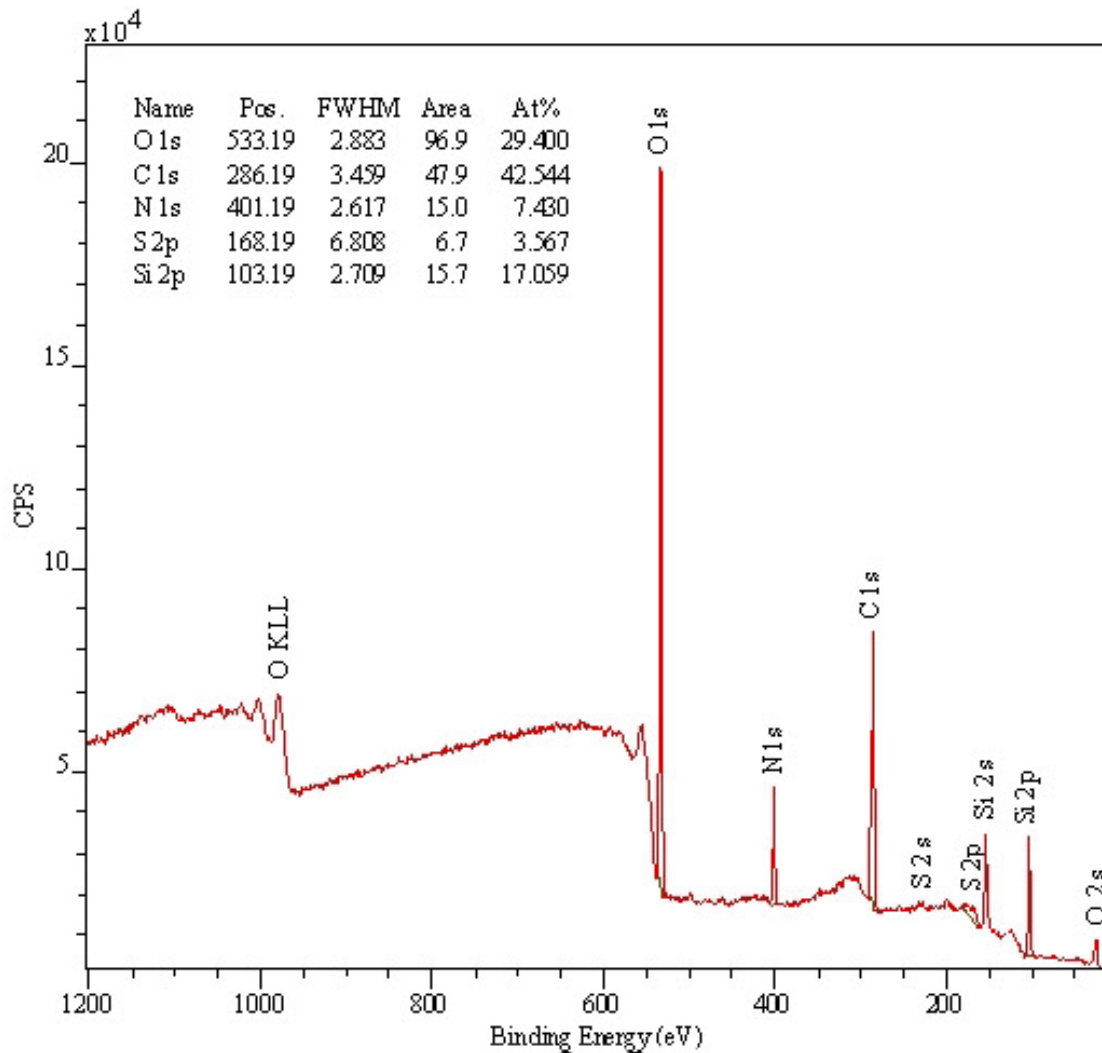


**Figure 2.8 XPS survey spectrum of a GMBS-modified surface covalently linked with FN protein. The inset table provides columns of information about the type of photoelectron detected, the binding energy (eV), the full-width at half-maximum of the fitted peak (eV), the numerically integrated peak area (arbitrary units), and the calculated atomic percent of the species (%), using literature values for the elemental attenuation factors.**

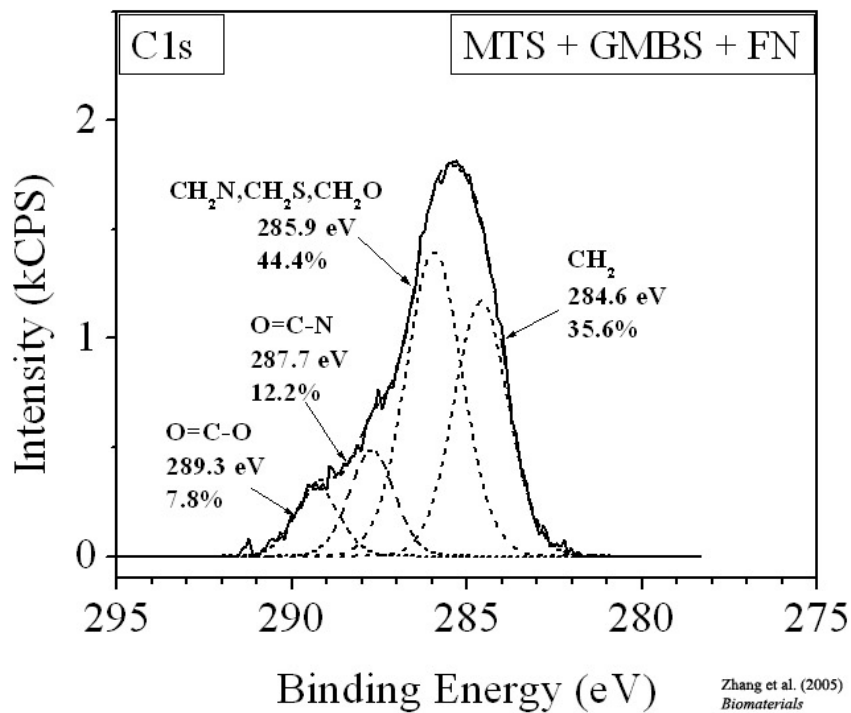


**Figure 2.9 XPS high-resolution spectrum of the C1s region of a substrate modified with covalently linked fibronectin.** (Reprinted from Zhang et al. (2005) *Biomaterials*)

However, the XPS is not without its limitations. As seen in Figure 2.9, chemical state structures that closely resemble each other can have very similar binding energies. This makes it very hard to resolve these peaks (i.e. -CH<sub>2</sub>N-, -CH<sub>2</sub>S-, -CH<sub>2</sub>O-), leading to spectral overlap. In non-conducting or insulating samples, which include most biological and organic substrates, the continuous emission of photoelectrons from the sample's surface creates a positive charge zone, referred to as charging. This results in peaks shifting to higher binding energy values on the order of several electron volts. The XPS is equipped with a low-energy electron flood gun that delivers electrons to the surface, enabling neutralization of surface charge. However,

if additional peak shifting is necessary, this can be accomplished using XPS spectral processing software.

Overall, the XPS is a highly surface-sensitive tool that is capable of providing both qualitative and quantitative information about the chemical composition and structure of a surface. Used in conjunction with the TOF-SIMS, these two tools are the workhorses of the surface science community.

## **2.6 Applications of Surface Sensitive Techniques**

Contact angle, XPS, and TOF-SIMS techniques were all used as tools for verification of successful modification of the surfaces with the GMBS chemistry mentioned in Chapter 1. Additionally, XPS was used as a tool for quantifying the density of FN present on the modified substrates to ensure that a gradient was formed. TOF-SIMS imaging was used to verify successful patterning of the gradient samples. These results will be presented in more detail in Chapter 4. AFM was mainly used in the  $\mu$ CP research in imaging of the comb polymer patterned surfaces, with line profile analysis of the images providing data about comb polymer height. Further details for this study are provided in Chapter.

## Chapter 3

### CONTROLLING NEURON GROWTH USING COMB POLYMER PATTERNED SUBSTRATES VIA MICRO-CONTACT PRINTING

#### 3.1 Overview

Studying neuron growth on biomaterial bridging substrates requires substrates that have the ability to control and direct neuron growth, rather than allow uncontrolled axonal extension. Controlling neuron growth would increase the probability of successful reconnection of damaged pathways. Previous research in our group has found that micro-patterning of an amphiphilic comb polymer with polyethylene glycol (PEG) side chains (i.e.  $(\text{CH}_2\text{CH}_2\text{O})_n$ ) is effective in producing a chemoattractive/chemorepulsive substrate capable of controlling neuron growth. However, in these studies, the variable of comb polymer feature height has been neglected.

This chapter will provide a brief introduction to the micro-contact printing ( $\mu\text{CP}$ ) technique, as well as results of my research on controlling comb polymer feature height on patterned substrates before I began my work on patterned gradient substrates. This research on comb polymer feature heights was continued by an undergraduate researcher in the group, Heather Egolf-Fox, and has resulted in a paper on which I am a co-author, that is currently being edited for submission to the journal *Biomacromolecules*.

### **3.2 Introduction**

As a non-photolithographic technique<sup>107</sup>, micro-contact printing ( $\mu$ CP) involves use of a poly(dimethylsiloxane) (PDMS) stamp with micron-sized features. PDMS has been used extensively in  $\mu$ CP for its elastomeric properties. These properties allow the stamp to conform easily to the surface of a substrate, yet allow enough durability to be used over a long period of time without significant degradation.<sup>108</sup> PDMS is also favorable because its surface can be made to be chemically inert, ensuring that the desired chemistry to be patterned does not adhere to or react with the stamp surface. PDMS has the disadvantage that a cured polymer stamp also contains low-molecular-weight oligomers with sufficient vapor pressure to leach out and adsorb in a thin film on top of surfaces in an undesired manner, often without the knowledge of the experimenters. This will be addressed below.

In  $\mu$ CP, the PDMS stamp is coated, or “inked”, with the desired chemical to be patterned. Bringing the stamp into conformal contact with the surface allows transfer of the desired chemical in the shape of the pattern onto the surface. A second molecule can be added to uncontacted regions by “backfilling” with a solution of the secondary molecule (See Figure 3.1).

$\mu$ CP has been widely used in many areas of research, including studies of cell growth and migration on patterned surfaces.<sup>86, 109-114</sup> Some groups have utilized their protein(s) of interest as the “inking” solution for  $\mu$ CP.<sup>115-118</sup> However, our studies involve  $\mu$ CP of an amphiphilic comb polymer. The amphiphilic comb polymer’s design contains a polymethyl methacrylate-like (PMMA) backbone with polyethylene glycol (PEG) side chains (See Figure 3.2). PEG has been shown to resist protein attachment<sup>97, 119-123</sup> and cell adhesion.<sup>97, 124-126</sup> Pre-immersion in water is found to

reorient and/or hydrate the PEG side chains at the solid/water interface, drastically improving its protein resistive properties.<sup>127</sup>

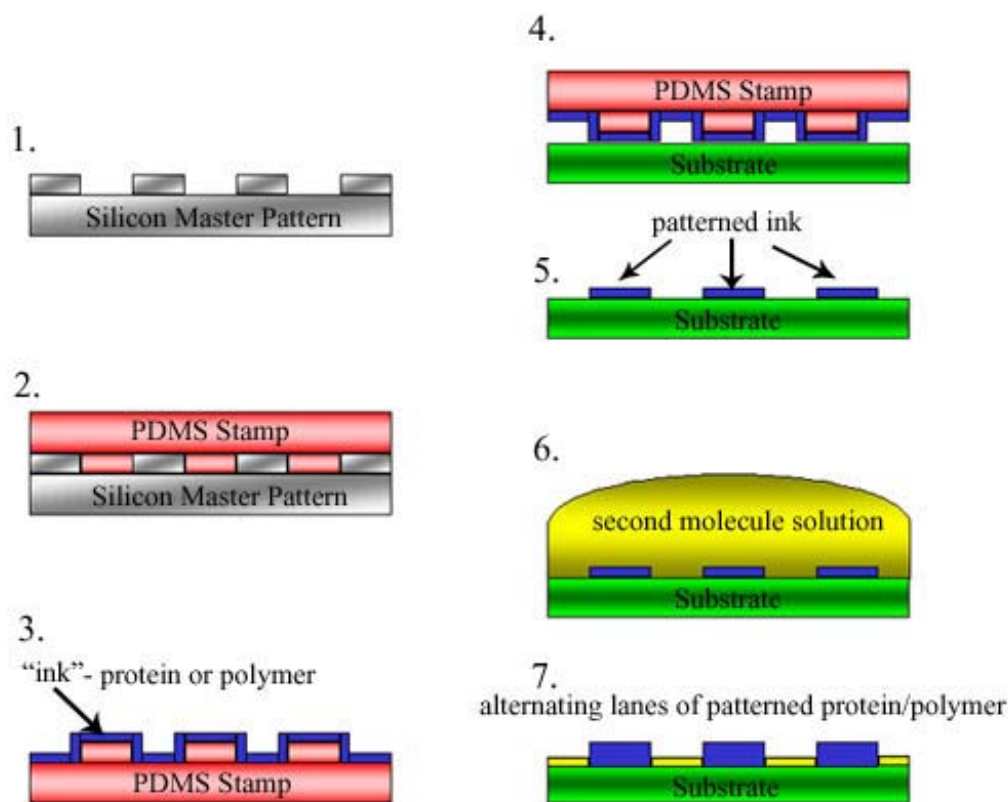


**Figure 3.1. Schematic diagram of micro-contact printing ( $\mu$ CP). 1) A silicon master is used to create a 2) PDMS stamp containing micron-sized features. 3) The PDMS stamp is "inked" with a molecule of interest and 4) brought into conformal contact with the substrate. 5) A pattern of the ink is generated on the substrate. 6) A solution of a second molecule can be backfilled onto the substrate, 7) filling in the unpatterned lanes of the substrate with the secondary molecule.**

Our group's recent studies of neuron growth on patterned surfaces with alternating lanes of comb polymer and fibronectin have shown the comb polymer's effectiveness in limiting neuron growth to only the lanes containing fibronectin.<sup>52, 86</sup> However, the measured height of comb polymer features in these studies was found to be almost  $600 \pm 150$  nm. A recent study indicates that the ends of extending neurites average  $385 \pm 193$  nm in height, while growth cones average only  $260 \pm 176$  nm.<sup>79</sup>

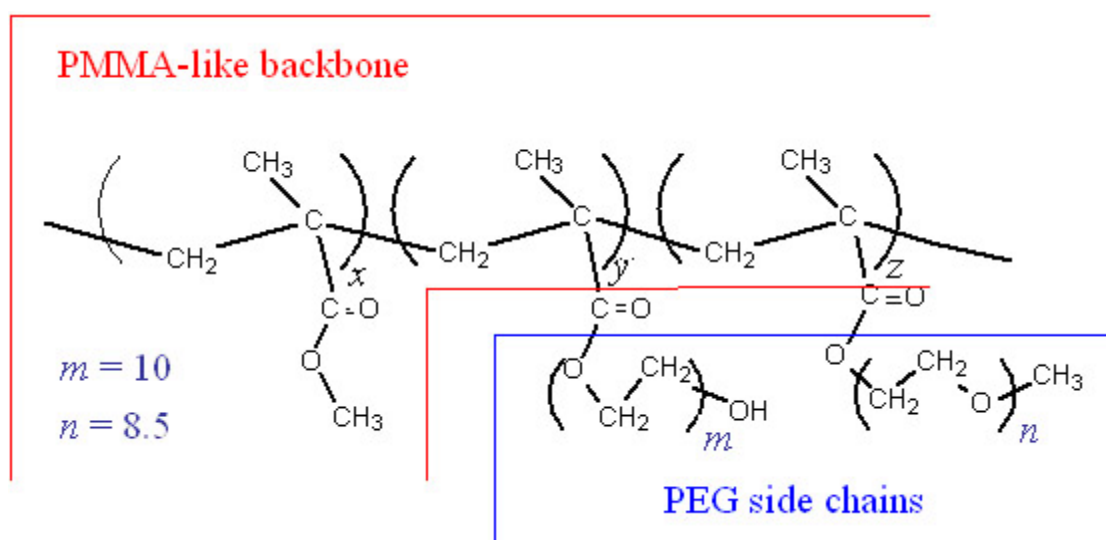


**Figure 3.2. An amphiphilic comb polymer containing a PMMA-like backbone with PEG side chains.**

With comb polymer features twice the height of extending neurites and almost three times as large as neuron growth cones, it is hard to determine whether the comb polymer is acting as a chemical barrier or a topographical one. This “chemical vs. topographical” mechanism of action may confound the interpretation of the data obtained in recent studies. By reducing comb polymer feature heights to lower than

the height of the neuron growth cone, the “chemical vs. topographical” problem can be separated to provide a better understanding of the effectiveness of comb polymer in controlling neuron growth. In this study, comb polymer solution concentration and pressure applied via transfer weight were varied to determine their effects on comb polymer feature height.

### **3.3 Experimental**

Micro-contact printing ( $\mu$ CP) was used to pattern comb polymer lanes (40  $\mu$ m width) onto polystyrene dishes. The resulting patterned substrates were then imaged and analyzed using atomic force microscopy (AFM) to determine the effects of comb polymer solution concentration and transfer weight applied on comb polymer feature height. All AFM height measurements were repeated 10 times on a minimum of 3 samples for each sample condition. The mean feature height, plus or minus one standard deviation, is reported.

#### **3.3.1 Comb Polymer Synthesis and Characterization**

Comb polymer was prepared using previous methods<sup>86, 128</sup> involving free-radical polymerization of methyl methacrylate (MMA), poly(ethylene glycol) methacrylate (HPOEM), and poly(ethylene glycol) methyl ether methacrylate (POEM). MMA (11.2611 g, 111.4 mmol, 59.0 wt%), POEM (3.8640 g, 8.1 mmol, 20.5 wt%), HPOEM (3.8672 g, 7.4 mmol, 20.5 wt%), and azo(bis)isobutyronitrile (AIBN) (0.1276 g, 0.8 mmol) were combined in a 500-mL round-bottom flask with 350 mL anhydrous THF. The mixture was deoxygenated for 30 minutes using clean N<sub>2</sub> gas and refluxed for an additional ~20 hours at 75°C. Quenching of the polymerization reaction was accomplished by adding 50 mg MEHQ to the solution. The solution was

concentrated and precipitated twice into a 1200-mL petroleum ether/methanol mixture (8:1), and vacuum dried with stirring for a 24-hour period. Comb polymer was characterized using  $^1\text{H}$  NMR (300 MHz, Varian, CA) in  $\text{CDCl}_3$ : HPOEM, 6.13 ppm ( $\text{CH}_2=\text{C}$ , singlet (s), 1H), 5.58 ppm ( $\text{CH}_2=\text{C}$ , s, 1H), 4.30 ppm ( $\text{COOCH}_2$ ,  $J = 4.5$ , triplet (t), 2H), 3.65 ppm ( $\text{CH}_2\text{CH}_2\text{O}$ , multiplet (m), 40H), 1.95 ppm ( $\text{C}=\text{CCH}_3$ , s 3H); POEM, 6.13 ppm ( $\text{CH}_2=\text{C}$ , s, 1H), 5.58 ppm ( $\text{CH}_2=\text{C}$ , s, 1H), 4.30 ppm ( $\text{COOCH}_2$ ,  $J = 5.1$ , t, 2H), 3.65 ppm ( $\text{CH}_2\text{CH}_2\text{O}$ , m, 40H), 3.38 ppm ( $\text{OCH}_3$ , s, 3H), 1.95 ppm ( $\text{C}=\text{CCH}_3$ , s 3H); Comb polymer, 4.11 ppm ( $\text{COOCH}_2$ , s, 2H), 3.6–3.7 ppm ( $\text{CH}_2\text{CH}_2\text{O}$ , m, 52H), 3.35 ppm ( $\text{OCH}_3$ , s, 1.5H), 0.5–2 ppm ( $\text{CH}_2\text{CCH}_3$ , m, 42H). The NMR-derived final composition of the comb polymers was close to the feed ratio of monomers.<sup>129</sup>

### **3.3.2 Synthesis of PDMS Stamps**

A Sylgard silicon elastomer kit was used in creating PDMS stamps. Silicon elastomer and curing agent were mixed (10:1) together in a 100-mL high density polypropylene (HDPP) beaker, and degassed in a vacuum chamber with stirring for 1 hour. After degassing, the mixture was poured into polystyrene dishes containing face-up silicon microstamp master patterns. Master patterns were produced by standard photoresist techniques on silicon wafers at the Biomedical Microsensor Laboratory in North Carolina State University (BMMSL-NCSU). The polystyrene dishes were placed in a vacuum oven (VWR 1400E, Shelton Manufacturing Co., Cornelius, OR) and the stamps were vacuum annealed and polymerized at  $80^\circ\text{C}$  for 2 hours. The stamps were then peeled away from the silicon masters, resulting in features that are the negative of the master patterns. Excess PDMS was cut from the

sides using a razor blade. The stamps used in this study had features of 40- $\mu\text{m}$ -wide gaps and 40- $\mu\text{m}$ -wide stripes.

### **3.3.3 Patterning of Comb Polymer**

Comb polymer was dissolved in an ethanol/DI water mixture (8:2) in varying amounts to produce comb polymer solutions with final concentrations of 10, 20, 50, 80, 100, and 150 mg/mL. Prior to patterning, the PDMS stamps were ultrasonically cleaned (Branson<sup>®</sup> Ultrasonic Cleaner B2200R-1, Branson<sup>®</sup> Ultrasonics Corporation, Danbury, CT) in ethanol/DI water mixture (8:2) for 5 minutes and blown dry using clean compressed air. Stamps were plasma cleaned (Plasma Cleaner/Sterilizer PDC-32G, Harrick Scientific, Ossining, NY) for 2 minutes in order to increase hydrophilicity, improve wettability of the stamp surface, and remove low-molecular-weight PDMS contaminants.

Plasma-cleaned stamps were spin coated (P6204 Spin coater, Specialty Coating Systems, Inc., Indianapolis, IN) with 150  $\mu\text{L}$  of comb polymer solution at 2,750 rpm for 7 seconds. To ensure a uniform coat, the comb polymer solution was spread over the entire face of the stamp using the pipette tip prior to spin coating. Immediately after the spin coating process, the stamp was removed from the apparatus and brought into conformal contact with a PS surface. Since the solvent of the comb polymer solution evaporates quickly, and since the degree of solvent evaporation was shown to be a critical factor in the quality of the printed films, care was taken to standardize and keep constant the exact process and time elapsed. Varying weights (5, 10, and 20 g) were added to apply varying amounts of pressure when transferring the pattern. The patterned substrates were then annealed in a vacuum oven at 60°C for 24 hours.

The patterning process was repeated for all combinations of transfer weight and comb polymer solution concentration. Prior to reuse of any stamps, the stamps were re-rinsed and ultrasonically cleaned in the ethanol/DI water mixture indicated previously.

### **3.3.4 AFM Imaging and Analysis of Patterned Surfaces**

Patterned substrates were imaged on a Digital Instruments Multimode Atomic Force Microscopy (AFM) using tapping mode. Images were obtained in air, using a standard silicon tip (Veeco Nanoprobes, Inc.) calibrated at a frequency of 300 kHz with a scan rate of 0.375 Hz. Images were only minimally processed with first-order flattening to obtain accurate height data using Nanoscope III software (v5.12R3).

### **3.4 Results and Discussion**

After first-order flattening and processing of the AFM images, height data were obtained using line profile analysis. Feature height was defined as the distance from the baseline to the flattest part of the feature top. If the top of the feature was not flat, an *average* of the top plane was used in determining feature height, as shown in Figure 3.3.

Height data were collected and are presented in Figure 3.4. One immediately notices the trend in decreasing feature height as a function of comb polymer solution concentration. As the comb polymer solution concentration was decreased, feature heights were found to decrease. A second relationship was observed between feature height and transfer weight applied to the stamp. The data indicate that, in general, as transfer weight was decreased, comb polymer feature heights also

decreased across all concentrations. With careful control of the experimental parameters, it was possible to create reproducible feature heights as low as 60 nm.

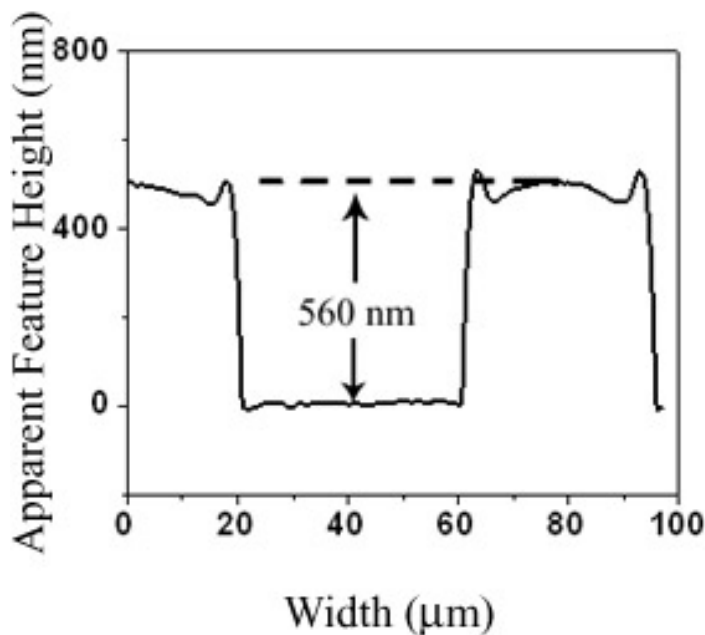
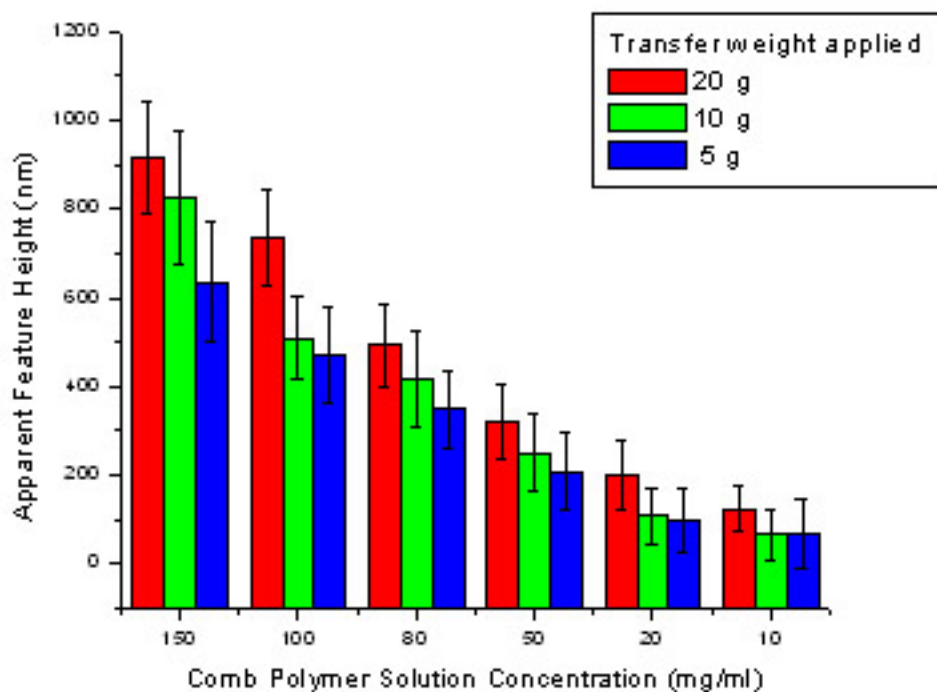


Figure 3.3 AFM line profile analysis of a patterned substrate. (**Reprinted from Egolf-Fox et al. (submitted) *Biomacromolecules***)

### **3.5 Conclusions and Suggested Future Studies**

Definite trends were observed in the effects of both comb polymer solution concentration and transfer weight on the apparent feature height. Results indicate that comb polymer feature heights can be controlled and decreased to ~60 nm. Patterned substrates with such low feature heights would be beneficial for neuron growth studies. With feature heights only a fraction of the height of neuron growth

cones, it allows us to study the neuron growth and determine if neurons can cross over the comb polymer.



**Figure 3.4. Apparent Feature Height as Effected by Transfer Weight and Comb Polymer Solution Concentration.**

This research was followed up by a member of our research group, Heather Egolf-Fox, and has yielded many significant findings that are reported in a publication on which I am a co-author.<sup>130</sup> The effects of comb polymer solution

concentration and transfer weight on feature height were confirmed to have statistical significance. Feature heights could be well controlled and samples could be patterned with feature heights as low as ~50 nm. In addition, tapping mode AFM performed in fluid found no significant difference in feature heights when compared to measurements taken in air. This is an important observation, as it is necessary to perform live neuron growth studies in a fluid medium. Preliminary neuron growth studies indicate that laminin/comb polymer patterned substrates with feature heights as low as ~90 nm effectively restrict neuron growth to within laminin lanes. Even at lower feature heights the neurons were unable to cross over the comb polymer into other lanes, indicating the comb polymer's effectiveness as a chemical barrier. However, more neuron growth studies are necessary to see if the findings are reproducible before an answer to the "chemical vs. topographical" problem can be confirmed.

## Chapter 4

### GENERATION OF GRADIENTS OF FIBRONECTIN ON PATTERNED SURFACES FOR NEURON GROWTH STUDIES

#### 4.1 Overview

As mentioned previously in Chapter 1, a fundamental question about the interaction between neurons and underlying ligands is how neuron outgrowth is affected by ligand density. In order to answer this question, gradient samples were created with changing ligand density for neuron growth studies. This chapter focuses on generation and characterization of these gradient surfaces for future neuron growth studies.

#### 4.2 Introduction

As early as 1928, Cajal suggested that axons were guided toward their destinations by attractive and repulsive chemical cues.<sup>131</sup> Findings of several groups support Cajal's theory, as neuron growth cones are found to sample the environment and turn in response to different guidance cues.<sup>132-137</sup> Cell migration or growth in response to chemoattractive and chemorepellent cues is referred to as *chemotaxis*, and various studies have been performed to identify chemical cues and factors for their possible roles in chemotaxis.<sup>132, 133, 138-151</sup>

Cells do not merely respond to these chemical cues, but to changes in the concentration of these cues in the form of an increasing gradient.<sup>136, 147, 152-158</sup> Cell movement and growth along a chemical gradient is referred to as *haptotaxis*,<sup>99, 154, 159</sup>

and evidence from RNA-tagging experiments has indicated that such chemical gradients are expressed in nature.<sup>140, 142</sup>

Two competing theories exist on how neurons will respond to chemical gradient surfaces. One theory is that neurons will reach maximal growth rates at intermediate ligand density and decrease with further increases in ligand concentration.<sup>80</sup> The decrease in growth rate is thought to be due to the overabundance of ligands on the surface, making it harder for the neuron growth cone to disengage from the bound ligands and continue growth. A second theory suggests that the neuron is more adaptive to its environment. Preliminary neuron studies have shown that axonal extension on laminin substrates reached a maximum rate and seemed to plateau and maintain that rate, regardless of increases in laminin concentration.<sup>81</sup> This theory argues that the neuron can sense changes in the environment and is able to regulate receptor expression accordingly.

Studies suggest that several factors must be taken into account when creating gradient surfaces, such as the slope of the gradient<sup>153, 160-163</sup> and its wettability.<sup>164-167</sup> Various methods of producing gradients have been developed including: microfluidic networks<sup>138, 168-171</sup>, micro-pipetting/pumping of diffusible cues<sup>137, 143, 144, 153, 155, 156, 158, 172, 173</sup>, diffusion methods<sup>161, 166, 174</sup>, cross diffusion of alkanethiols on gold surfaces<sup>99, 175-180</sup>, corona discharge treatment<sup>181, 182</sup>, under-agarose method<sup>183-185</sup>, shadow mask deposition techniques<sup>97, 159, 163</sup>, electrochemically-derived gradients<sup>186-188</sup>, and various others<sup>147, 154, 189-198</sup>.

Although the methods listed above are capable of producing gradient surfaces, most of the techniques are rather costly, time consuming, and complex. However, simpler methods for producing gradients do exist<sup>193, 196</sup>. This thesis stands

to expand on the repertoire of simple and inexpensive methods for designing patterned gradients by studying FN density on a substrate as a function of incubation time. The method uses a motorized linear-motion device to vary the interplay of surface reaction kinetics and immersion time.

### **4.3 Experimental**

Surfaces were first modified using GMBS crosslinker chemistry<sup>60</sup> and prepared for FN incubation, as described in previous chapters. Gradients of fibronectin were generated on the substrate by changing the incubation time using a custom-built motorized linear-motion gradient device. For patterned gradient samples, a GMBS-modified substrate was first patterned with an amphiphilic comb polymer followed by generation of the FN gradient. Patterned surfaces are necessary in order to control neuron growth and provide a more accurate measure of the gradient's contribution. Surface preparations and modifications were characterized using contact angle, XPS, and TOF-SIMS. Additionally, XPS was also used for quantification purposes to ensure gradient formation. Preliminary neuron growth was examined using optical microscopy.

#### **4.3.1 Surface Modification Using GMBS Crosslinker Chemistry**

Surface modification procedures from our group's prior research were followed when modifying the substrate with GMBS crosslinker chemistry<sup>52</sup>. Glass cover slips (rectangular, 11 × 22 mm) (Thomas®) were immersed in a Piranha solution (7:3: (v/v) H<sub>2</sub>SO<sub>4</sub>: H<sub>2</sub>O<sub>2</sub>) for 30 minutes. **CAUTION: Piranha solution has highly acidic and oxidizing properties. Facemasks, full protective gloves, and a lab coat are recommended for proper safe handling.** Surfaces were rinsed with

distilled water 3-5 times and underwent five 10-minute sessions of ultrasonic cleaning in 18 M $\Omega$  cm water (Branson<sup>®</sup> Ultrasonic Cleaner B2200R-1, Branson<sup>®</sup> Ultrasonics Corporation, Danbury, CT). The surfaces were then covered with aluminum foil and dried on a hotplate at 140°C for 1 hour.

These clean glass surfaces were transferred into a glove bag under an inert atmosphere (N<sub>2</sub>) and placed in a 2% solution of 3-Mercaptopropyltrimethoxysilane (MTS) (Gelest) for a period of 2 hours. The “thiolated substrates” were removed from the MTS solution, rinsed in dry toluene, and allowed to air dry.

N- $\delta$ -maleimidobutyryloxy succinimide ester (GMBS) (Aldrich) was dissolved in a minimum amount of dimethylformamide (DMF) (Aldrich) and diluted with absolute ethanol (VWR Scientific) to a final concentration of 2 mM. The MTS-treated substrates were then placed in the GMBS solution for 1 hour, and then washed with absolute ethanol three times.

#### **4.3.2 Generation of Fibronectin Gradients on Unpatterned Samples**

Fibronectin (FN) was obtained from Calbiochem and diluted using phosphate-buffered saline (PBS) to a 50  $\mu$ g/ml solution. The FN solution was warmed to 37°C prior to use, and transferred to a custom-built multiwell glass dipping container consisting of several low-volume chambers to minimize the volume of expensive protein or peptide solution required. GMBS-modified substrates were placed in a custom-built sample holder of a custom-built motorized linear-motion device and dipped into the FN solution at a defined rate (See Figure 4.1).

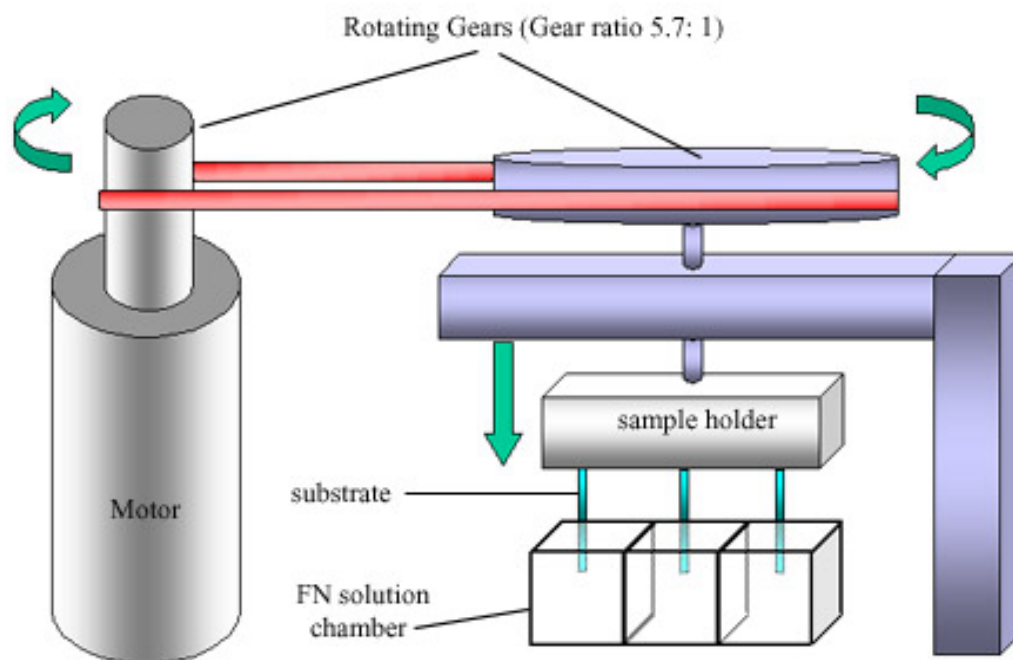


**Figure 4.1 Schematic diagram of custom-built motorized linear-motion gradient device.**

As shown in Figure 4.1, this device consisted of a motor (Company, model number, city, etc.) powered by a variable source of AC voltage (Variac, model number, etc.), turning a small gear. The small gear was in turn connected to a large gear, by means of a rubber band, in a diameter ratio of 5.7 to 1.0. The large gear on the sample side of the apparatus was directly connected to a drive thread having 80 threads per inch, or 317.5 microns per turn. Thus, by adjusting the rotational rate of the motor to approximately 1 rotation per minute, it was possible to achieve a linear drive rate of approximately 5.3 microns per second, resulting in the reactive GMBS surface being increasingly submerged at this rate. Because the reaction kinetics of a solution of a given concentration of FN protein with a reactive GMBS surface are known<sup>127</sup>, one can easily calculate the resulting local concentration of FN as a

function of distance along the immersion direction. Such a situation is depicted schematically in the red curve of Figure 4.2, resulting in a continuous concentration gradient.

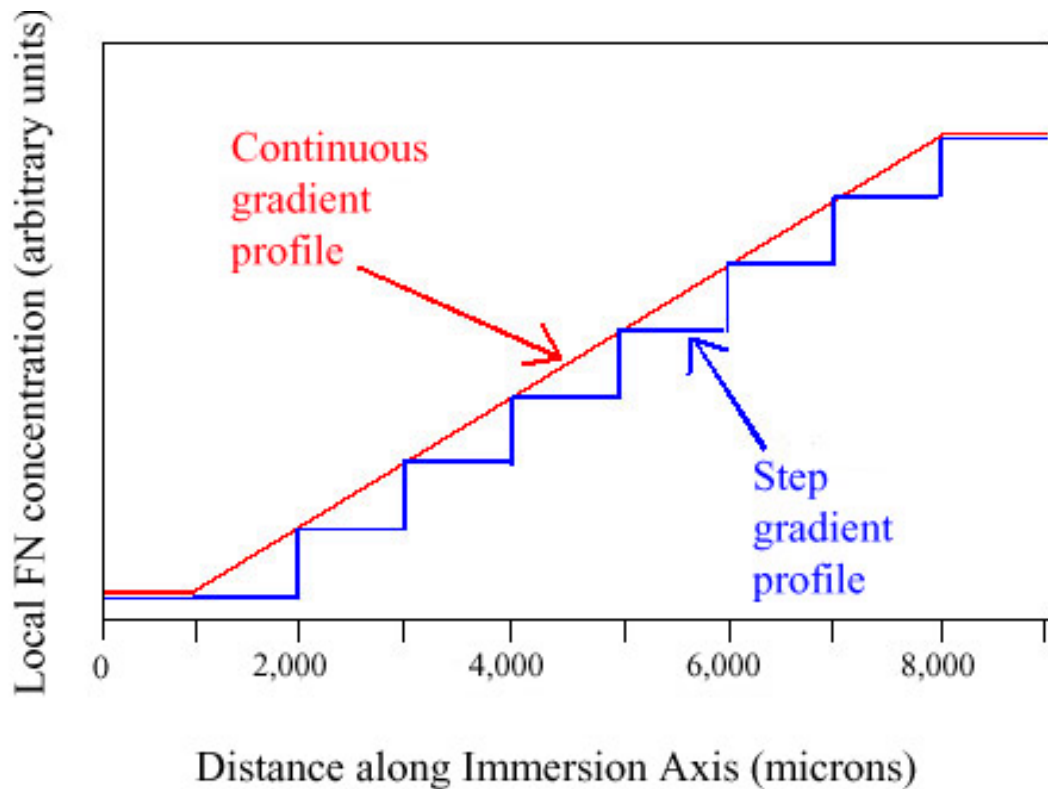


**Figure 4.2 Generation of continuous and step gradient profile surfaces.**

Alternatively, the blue curve of Figure 4.2 depicts the type of immersion program employed in the present studies. The sample was rapidly immersed to a known, constant depth for a fixed time, the hold time, then advanced to the next depth for the same hold time, and so on. It was hypothesized that since the motion to the next depth occurs on a time scale that is two orders of magnitude shorter

than the duration of the hold time, a step-like local concentration profile of FN existed on the surface. The schematic diagram of Figure 4.2 (blue curve) depicts eight 1-mm-wide stripes of constant local FN concentration. Although the *relative* position resolution of the gradient apparatus is a few microns, and although the *relative* position resolution of the analytical techniques is approximately one micron (XPS and TOF-SIMS) or one nanometer (AFM), the ability to locate an absolute position is a few tens of microns at present. Therefore, we opted to create relatively wide stripes (1 mm) of constant local FN concentration initially. The step-size of our custom-built gradient device was on the order of several microns.

Gradients were produced by immersing the pre-coated surfaces into the FN solution to a defined distance and stopping to allow the submerged portion to incubate for a certain length of time. The sample was then lowered further and the process repeated. This procedure was done several times to produce samples with incubation times ranging from 5-120 minutes. Gradient samples were then rinsed 3 times with PBS buffer, 3 times with distilled water and allowed to air dry. In addition to creating gradients using short incubation intervals (e.g. 10-minute intervals), longer incubation intervals were also used (e.g. 30-minute intervals) in order to test results from previous studies indicating neuron growth is affected by a gradient's slope.<sup>153,</sup>

160-163

### **4.3.3 Generation of Patterned Gradient Samples**

In addition to creating FN gradients on unpatterned GMBS surfaces, patterned gradient surfaces were also created. GMBS-modified substrates were first patterned with an amphiphilic comb polymer using the micro-contact printing ( $\mu$ CP) technique discussed in Chapter 3. An elastomeric PDMS stamp was first spin-coated

with 150  $\mu\text{L}$  of a 100-mg/ml solution of comb polymer. The stamp was then brought into conformal contact with the GMBS-modified surface to transfer the pattern. Patterning of the substrates resulted in alternating lanes of comb polymer (40 microns wide) and GMBS (40 microns wide). Patterned surfaces were annealed in a vacuum oven at 60°C for 24 hours and then immersed in deionized water for 2 hours to enhance the comb polymer's protein resistivity. The orientation of the printed pattern relative to the immersion axis can be varied to produce different types of gradients, as depicted in Figure 4.3.

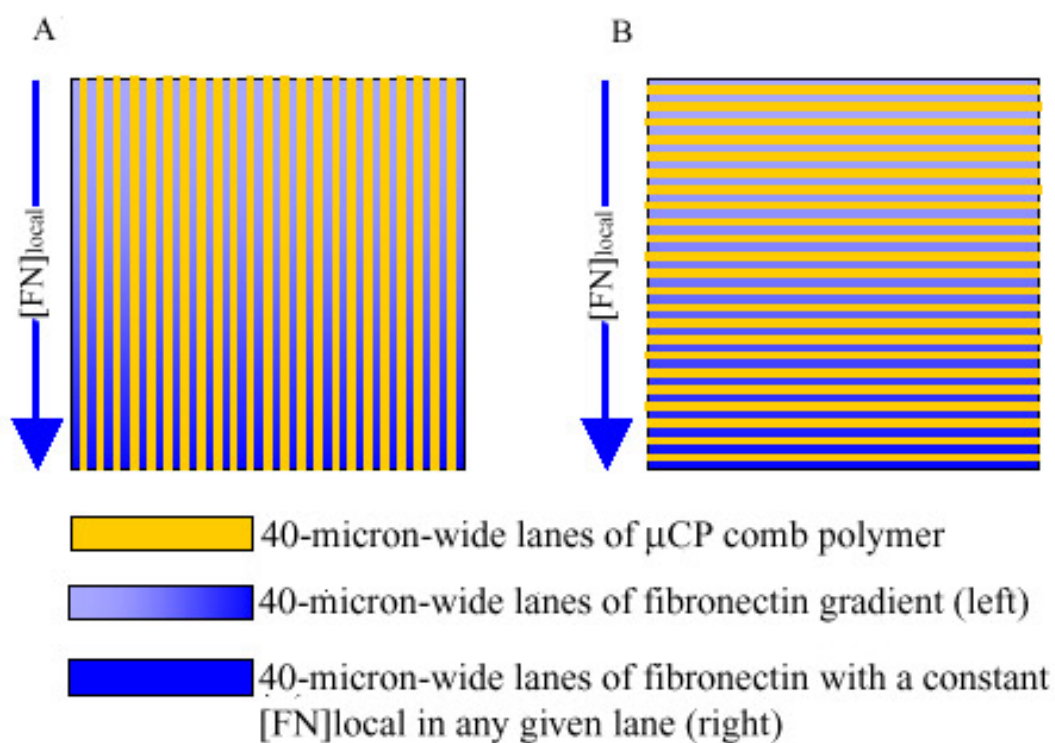


**Figure 4.3 Orientation of the printed pattern relative to the immersion axis, resulting in a) vertical, and b) horizontal gradients of fibronectin.**

When the axis of immersion is parallel to the axis of the stripes, as in Figure 4.3.A, a series of stripes, each separated by a comb-polymer stripe and each with the same FN gradient in the vertical direction is produced. When the axis of immersion is perpendicular to the axis of the stripes, as in Figure 4.3.B, a series of stripes, each separated by a comb-polymer stripe and each with a different but constant local FN concentration is produced.

#### **4.3.4 Contact angle measurement**

Videomicroscope images of sessile drops were obtained using a contact angle instrument (FTA125, First Ten Ångströms, Portsmouth, VA) with an RS170 camera. Sessile drop images were obtained through movie capture in order to maintain consistency in contact angle determination. In these experiments, contact angle was defined as the first image in which the drop stabilizes after detachment from the syringe. Contact angle measurements were calculated using FTA32 v2.0 software. The liquid used in these contact angle measurements was deionized water obtained through Milli-Q filtration with a measured resistivity of 18 MΩ cm. All reported contact angles are the averaged result of 5 replicate measurements made at different locations on 20 different samples, with errors reported as one standard deviation.

#### **4.3.6 TOF-SIMS**

Static TOF-SIMS spectra and images were performed on an instrument (TOF-SIMS IV, ION-TOF, Münster, Germany) using a 25-keV monoisotopic  $^{69}\text{Ga}^+$  primary ion beam generated by a  $\text{Ga}^+$  ion gun. High mass resolution ( $m/\Delta m=10,000$ ) was obtained using “bunched mode” of the TOF-SIMS instrument. The typical target current of the primary  $\text{Ga}^+$  beam in bunched mode was  $\sim 1$  pA, with a prebunched

pulse width of 25 ns. Following bunching, the arrival pulse width, as judged by the FWHM of the H<sup>+</sup> peak, was typically 700 ps. For nonimaging spectral acquisition, the raster area of the Ga<sup>+</sup> ion gun was 500 x 500 μm<sup>2</sup>, and the raster resolution was 128 x 128 pixels. For imaging applications, the raster area was reduced to 384 x 384 μm<sup>2</sup>, in order to attempt to match the pixel size with the Ga<sup>+</sup> ion beam spot size (i.e., the Ga<sup>+</sup> ion beam spot size was adjusted to be approximately  $384 \div 128 \approx 3$  μm). Low-energy electrons (~20 eV) were supplied by a pulsed electron flood gun for charge compensation of the insulating samples. All primary Ga<sup>+</sup> ion fluences were below the threshold ( $1 \times 10^{13}$  ions cm<sup>-2</sup>) for static SIMS.

#### **4.3.5 XPS**

XPS analysis was performed on an ESCALab 250i-XL electron spectrometer (VG Scientific, UK) with a monochromatic Al Kα(1486.6 eV) X-ray source. Survey spectra and high-resolution spectra were obtained using pass energies of 100 and 20 eV, respectively. An average of 20 to 25 scans were collected for each high-resolution spectrum presented. The charging of the sample was compensated by use of a low-energy electron flood gun, typically operated at 6.0 eV and ~170 nA cm<sup>-2</sup> sample flux. All peaks were shifted accordingly by the amount required for the methylene component of the C 1s peak to be centered at 284.6 eV, as is customary, and all spectra were presented and analyzed with a Shirley-type background removed. Peak fitting and quantification were performed with both VG Eclipse v3.1 software (VG Scientific, UK) and CasaXPS v2.2.24 software(Casa Software Ltd., UK).

#### **4.3.7 Neuron plating**

Individual dorsal root ganglia (DRG) were removed from the spinal column of P1 Sprague-Dawley rats and the nerve roots were stripped. The ganglia were digested first with 0.25% collagenase for 20 minutes and then 0.025% trypsin-EDTA for 3 minutes. After each digest the tissue was titrated and centrifuged for 5 minutes at 1,000 rpm. The cells were then plated onto the patterned gradient surface. 2 mL of cell culture medium was added to each dish to support the neuron growth. The cell culture medium was composed with DMEM-F12 medium supplemented by 1% N2-Supplement, 0.1% ARAC, 10 ng/mL nerve growth factor, and 0.5% P/S (Penicillin/Streptomycin). The samples were incubated at 37°C with 5.0% CO<sub>2</sub>.

Cell growth was observed with a Nikon Eclipse TE2000-S Inverted Microscope equipped with a Roper Scientific Photometrics Camera, and images were analyzed using Image Pro Express 4.0 Software.

#### **4.4 Results and Discussion**

For this study, XPS and TOF-SIMS analysis were mainly used on characterization of FN gradients on the unpatterned and patterned surfaces, skipping over characterization of the GMBS crosslinker chemistry. Previous research<sup>52</sup> in our group has already characterized each step of the GMBS scheme by using XPS, contact angle, and TOF-SIMS analysis and shown this chemistry protocol to be highly reproducible. However for each preparation, in order to verify that the GMBS chemistry was attached to the substrates prior to patterning and FN incubation, contact angle measurements were used as a quick check method.

#### **4.4.1 Contact angle measurements of the GMBS crosslinker chemistry**

Contact angles were used in order to ensure the GMBS crosslinkers were attached properly to the surfaces prior to FN incubation. Contact angles were repeated several times for each sample and are summarized in Table 1. After cleansing in Piranha solution, the glass surfaces exhibited a contact angle of  $13.9 \pm 1.3^\circ$ . After 2 hours of immersion in the MTS solution, the surfaces exhibited a contact angle of  $59.7 \pm 1.6^\circ$ . Finally, the contact angle measured following 1 hour of immersion in a GMBS solution was  $50.8 \pm 1.4^\circ$ . These results were nearly identical to those in our previous research<sup>52</sup>, and interpreted as successful modification of the surfaces for use in subsequent steps before FN incubation.

**Table 4.1. Contact angle measurement comparison for each step of the GMBS Crosslinker Chemistry**

| <b>Surface modification</b>     | <b>Measured contact angle (°)</b> |
|---------------------------------|-----------------------------------|
| <i>Piranha-cleaned glass</i>    | $13.10 \pm 1.2$                   |
| <i>After reaction with MTS</i>  | $60.82 \pm 1.4$                   |
| <i>After reaction with GMBS</i> | $50.93 \pm 1.6$                   |

#### **4.4.2 TOF-SIMS Characterization of Unpatterned and Patterned FN Gradients**

TOF-SIMS analysis was used as a complementary method to XPS for verification of the attachment of FN to the substrates. The positive-ion spectrum of an unpatterned FN-gradient surface is presented in Figure 4.4. FN attachment was verified by the presence of peptide bond ( $\text{O}=\text{C}-\text{N}$ ) and amino acid residue peaks [such as the immonium ion,  $[\text{H}_2\text{N}=\text{CH}-\text{R}]^+$ ,  $m/z = (29+\text{R})$ ] present in the spectrum.

In addition, TOF-SIMS imaging was used to verify successfully patterned gradients. In doing so, the imaging helped discover an inherent flaw in the methods

used to produce a FN gradient (See Figure 4.5). In this study, GMBS/comb polymer surfaces were first immersed in water for 2 hours to allow the vacuum annealed comb polymer to rehydrate/reorient to repair its protein resistive properties.<sup>127</sup>

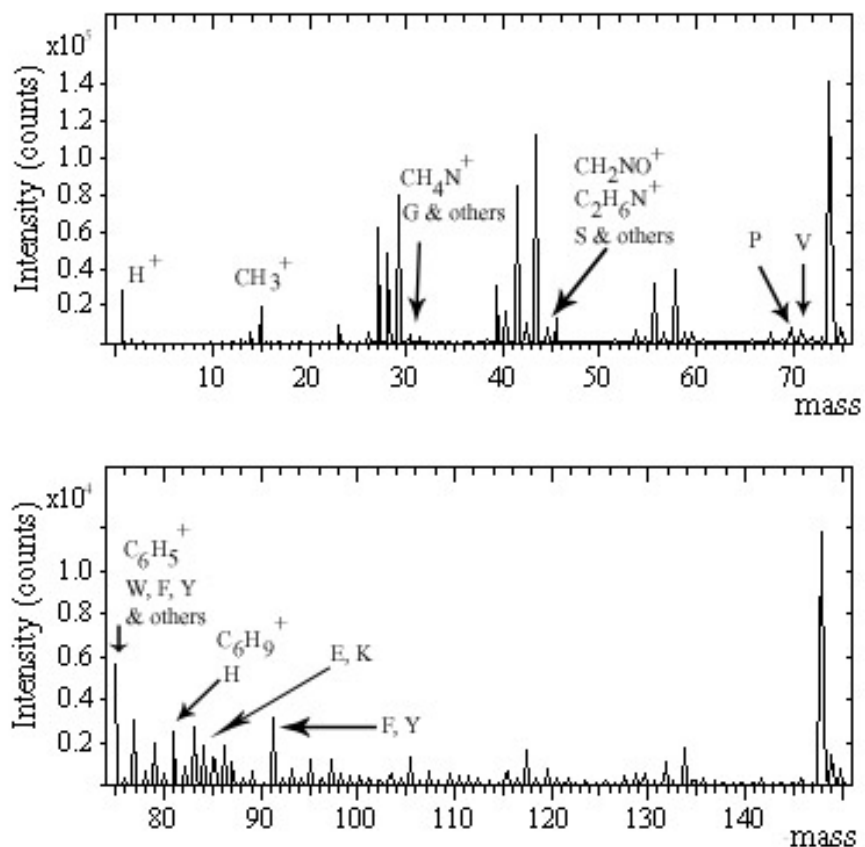
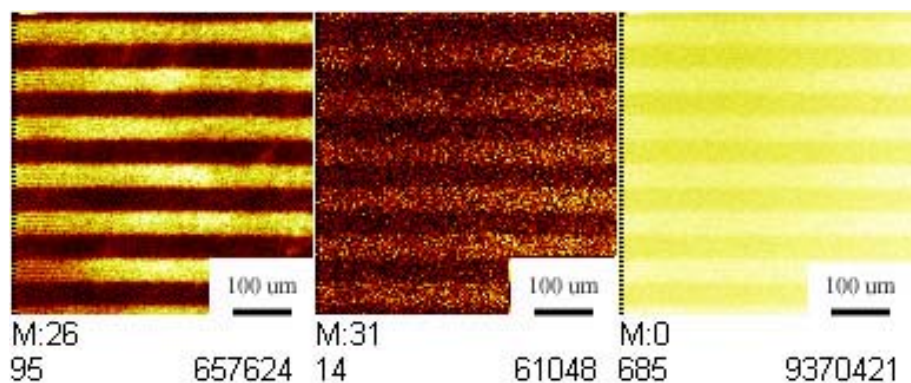
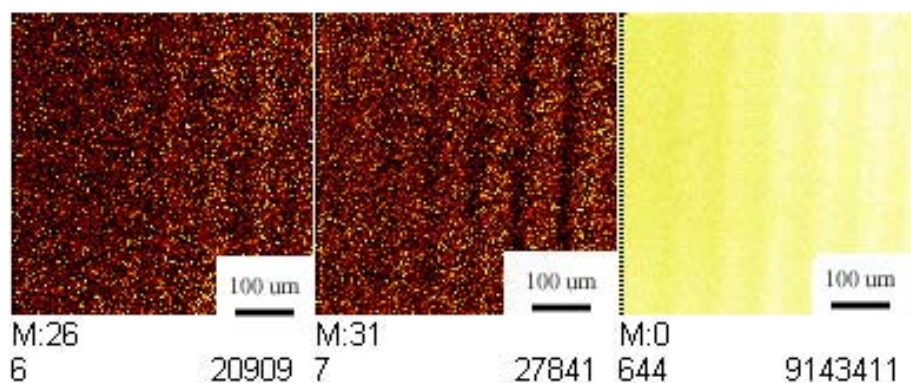


**Figure 4.4 Positive-ion TOF-SIMS survey spectrum for a GMBS +FN modified gradient. Several amino acids are indicated by the labeled fragments, including: Amino acids Glycine (G), Serine (S), Proline (P), Valine (V), Tryptophan (W), Phenylalanine (F), Tyrosine (Y), Histidine (H), Glutamic acid (E), and Lysine (K).**

Then samples were mounted onto the sample holder and slowly dipped into the FN solution at defined speeds and intervals in order to create a gradient. As the incubation interval between sections of the gradient was increased, the remaining portion of the substrates remained in air longer, allowing the comb polymer to reorient to its original form.



a)



b)

**Figure 4.5 TOF-SIMS imaging of gradient substrates incubated in a solution of FN for a total of a) 15 minutes, and b) 120 minutes.**

As a result, comb polymer exposed to the air for too long was allowed to dry out and ineffective in resisting protein adsorption and the FN was able to adhere to both GMBS and comb polymer lanes alike.

#### **4.4.3 XPS Characterization of Unpatterned and Patterned FN Gradients**

XPS was used to characterize and quantify the production of a FN gradient on both unpatterned and patterned samples. A comparison of XPS survey spectra from gradient substrates created in 15 minutes and 120 minutes of total incubation is shown in Figure 4.6. The existence of nitrogen on the surface in both spectra were suggestive of successful attachment of FN to the surface

Additionally, high-resolution XPS spectra of the C1s region are shown in Figure 4.7(a), (b) for both samples. As seen in Figure 4.7, while the  $-CH_2-$  decreased from 52.626% to 38.658%, the peak indicative of the peptide bond ( $O=C-N$ ) experiences a rise in percentage from 8.854% to 19.268% as total incubation time in FN solution is increased from 15 minutes to 120 minutes. Both XPS high-resolution and survey spectra of the gradient substrates indicated that the FN surface concentration increased as incubation time increased.

In order to quantify the gradient more carefully, protein surface coverage was examined at different incubation times and analyzed using XPS. The ratio of atomic percentage of nitrogen to atomic percentage of oxygen was used here to represent relative protein coverage on the surfaces. This ratio was plotted as a function of incubation time (See Figure 4.8). In the unpatterned substrates, the surface concentration was found to steadily increase from 0-70 minutes of incubation time, after which the surface coverage seemed to plateau (See Figure 4.8a). Shown in Figure 4.8b, the surface concentration of FN follows a similar trend in the patterned samples.

However, patterned FN gradients showed continued increase in FN surface concentration. This is thought to occur as a result of two factors: 1) Patterning prior to FN incubation results in a decrease in overall percentage of nitrogen, as expected due to the partial surface coverage of comb polymer. 2) As discussed in the previous section with TOF-SIMS results, dipped samples contain an inherent flaw that allowed the comb polymer to return to its original form, becoming less effective at resisting protein adsorption. As a result, the continued increase in FN surface concentration of the patterned substrates after 70 minutes is thought to be due to FN continuing to adsorb on top of the comb polymer.

#### **4.4.4 Preliminary Neuron Growth Studies**

Due to time constraints, only preliminary neuron growth was studied on the patterned gradient surfaces. Due to the inherent flaw in the methodology of producing the gradient mentioned previously, FN was not restricted to within GMBS lanes but was also spread across the comb polymer. As a result, in some cases neurons were found to grow unrestricted in the lanes, growing on and across the comb polymer on most surfaces, as seen in Figure 4.9. Therefore, neuron growth measurements were not performed, as it is necessary to restrict the gradient to within lanes before accurate measurements can be taken.

#### **4.5 Conclusions/Future Studies**

Overall, the present study indicates that a fibronectin gradient can be successfully established on a GMBS-modified substrate by simply controlling the incubation time. This is a very simple and relatively inexpensive way of creating gradients compared to other methods used in the field.

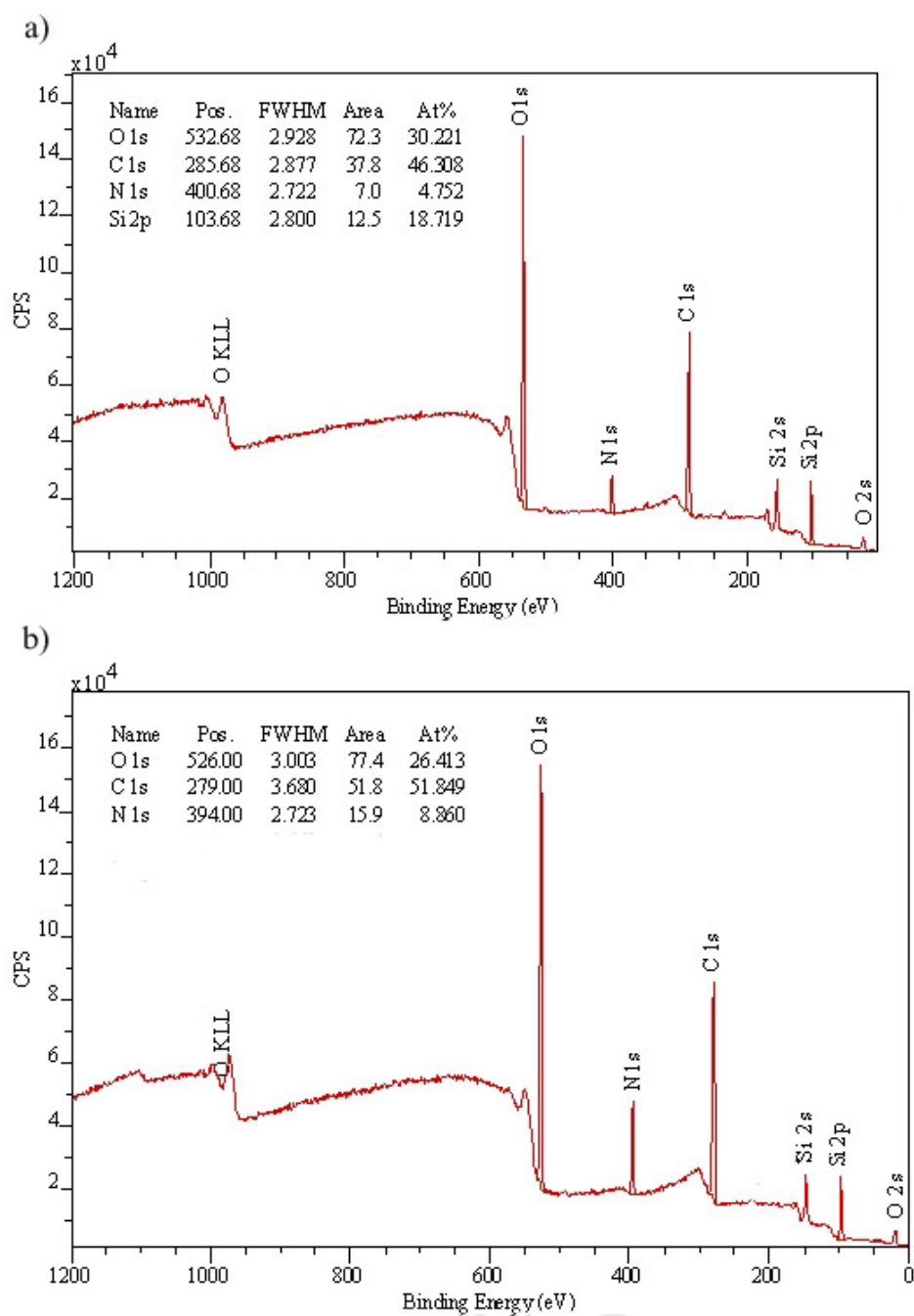


**Figure 4.6 XPS survey spectra of a GMBS-modified substrate incubated in a FN solution for a total of a) 15 mins, and b) 120 mins.**

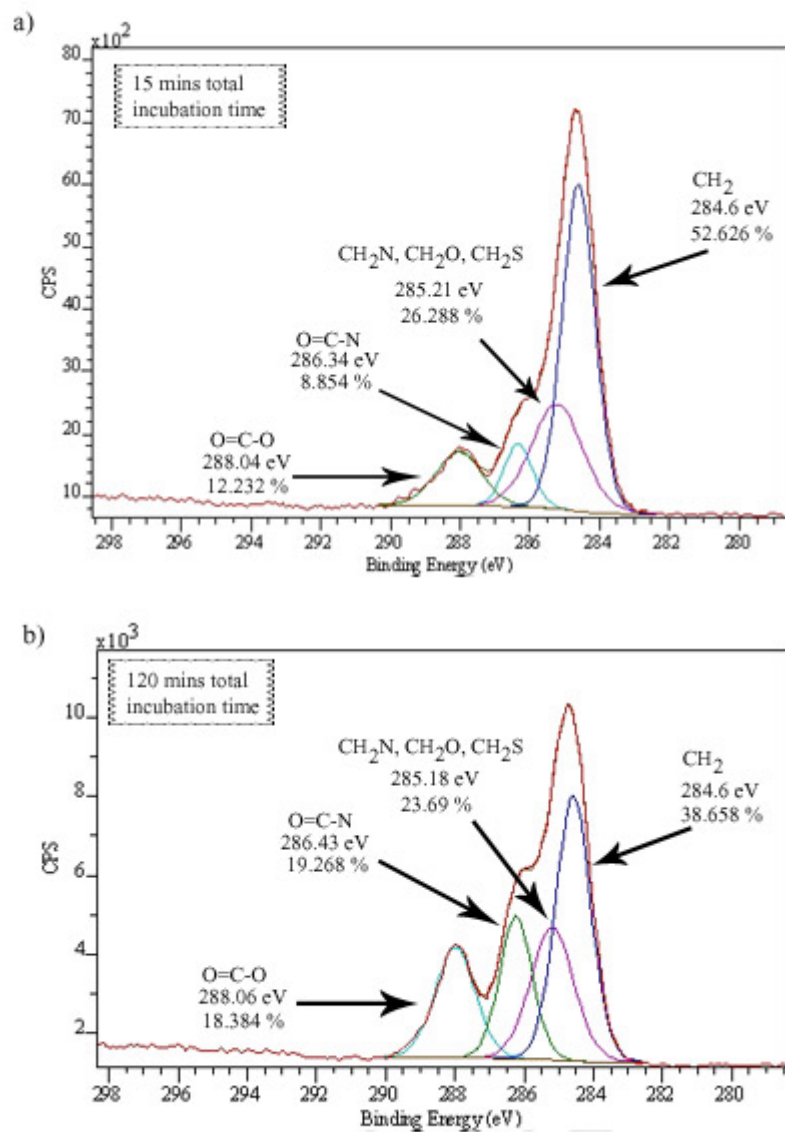


**Figure 4.7 XPS high-resolution spectra of the C1s region of GMBS-modified substrates incubated in FN solution for a total of a) 15 mins, and b) 120 mins.**

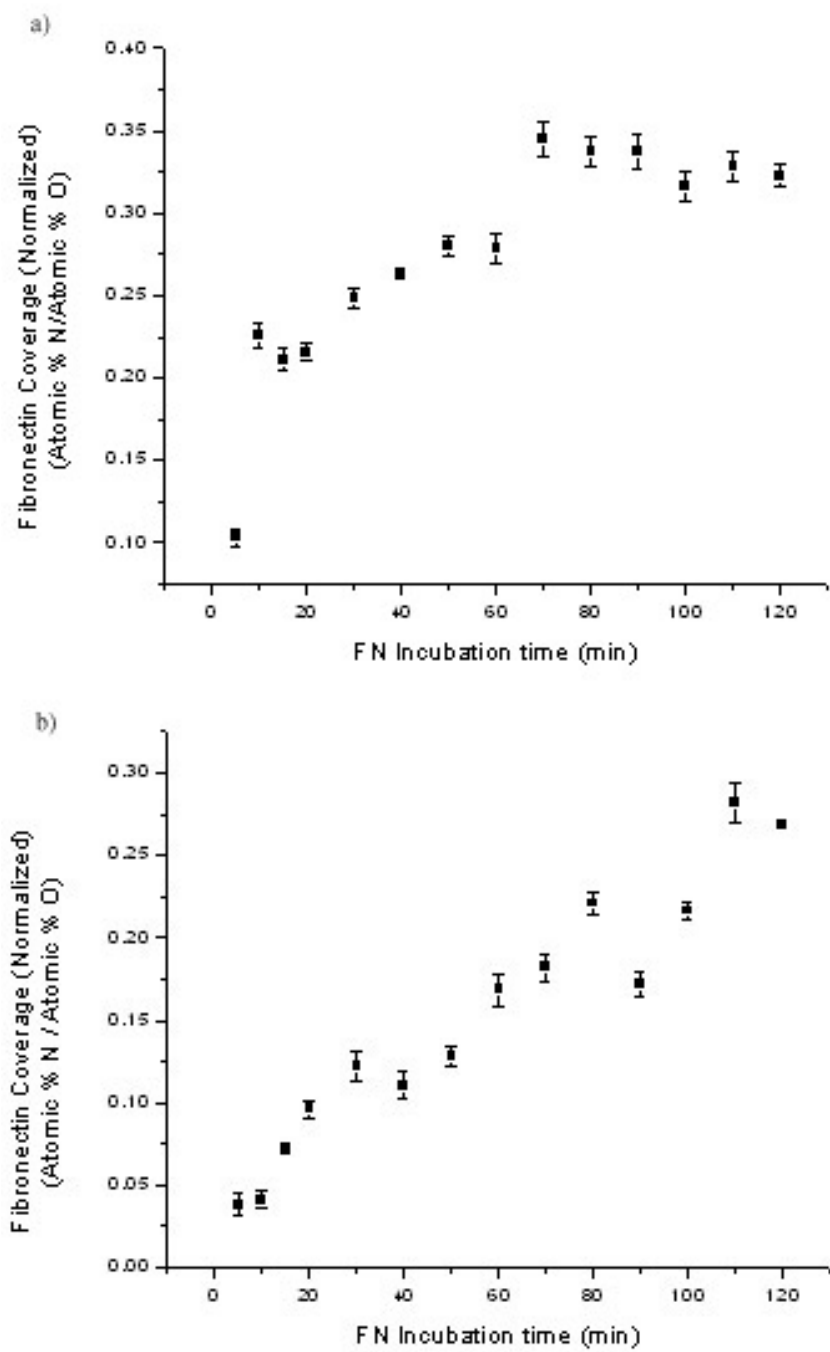


**Figure 4.8** Fibronectin surface coverage on: a) a control substrate, and b) a patterned substrate as a function of FN incubation time.

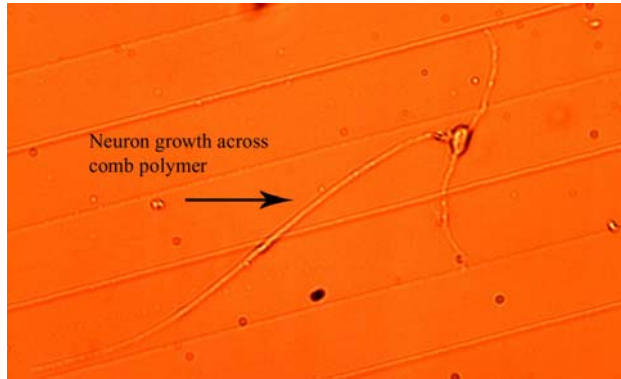


**Figure 4.9 Brightfield image of a neuron growing on and across a comb polymer lane.**

However, during the study several problems were observed involving the methodology. These problems must be resolved and controlled in order to proceed using this method for future gradient studies. While unpatterned gradients were made successfully, complications arose in the production of patterned FN gradients. In order to limit FN interactions with contaminants in the air, the gradients were made by dipping the substrates into the FN solution. While acceptable for creating patterned gradients with short incubation times and intervals, this method was ineffective in producing gradients with longer FN incubation intervals. By dipping the substrates over a length of time, the comb polymer on most parts of the surface will have dried out and reverted to its original form, reducing its effectiveness in resisting protein adsorption.

A more effective way to create these gradients in the future would be to do the reverse by pulling the samples out of the FN solution rather than dipping. By doing so, the comb polymer remains in solution for the majority of the experiment, and the portion of the sample exposed to air would already have FN adsorbed to

within the GMBS lanes. These “pull-out” experiments would have to be performed in a more carefully contained environment, by controlling factors such as temperature and humidity, in order to prevent the FN from reacting with any contaminants in the air.

Future success in creating patterned gradients by using this “pull-out” method would lead to further neuron growth studies on these gradient substrates. Only after the FN gradient is constrained to within GMBS lanes will we be able to accurately study its effects on neuron growth. Additionally, the comb polymer feature heights in the patterned gradient samples used in this study were not controlled, resulting in substrates with feature heights ranging from 600-800 nm. Once gradients can be created within the GMBS lanes, it would be beneficial to decrease the comb polymer feature heights to the height of the neuron growth cone. As mentioned in Chapter 3, comb polymer feature heights as low as ~90 nm were successful in limiting neuron growth to within lanes of laminin. However, it would be interesting to see how the combined effects of low feature heights and an increasing gradient would affect neuron growth.

## References

1. Healthgate/HDI About Spinal Cord Injuries.  
<http://www.spinalcord.org/html/injury.php> (Accessed July 5th, 2005),
2. Kandel, E. R.; Schwartz, J. H.; Jessell, T. M., *Essentials of Neural Science and Behavior*. McGraw-Hill: New York, 1995.
3. Skene, J. H. P., Growth-associated proteins and the curious dichotomies of nerve regeneration. *Cell* 1984, 37, (3), 697-700.
4. Skene, J. H. P.; Virag, I., Posttranslational membrane attachment and dynamic fatty acylation of a neuronal growth cone protein. *Journal of Cell Biology* 1989, 108, (2), 613-624.
5. David, S.; Aguayo, A. J., Axonal elongation into peripheral nervous system "bridges" after central nervous system injury in adult rats. *Science* 1981, 214, (4523), 931-3.
6. Davies, S. J.; Fitch, M. T.; Memberg, S. P.; Hall, A. K.; Raisman, G.; Silver, J., Regeneration of adult axons in white matter tracts of the central nervous system. *Nature* 1997, 390, (6661), 680-3.
7. Franklin, R. J.; Barnett, S. C., Olfactory ensheathing cells and CNS regeneration: the sweet smell of success? *Neuron* 2000, 28, (1), 15-8.
8. Kwon, B. K.; Tetzlaff, W., Spinal cord regeneration: from gene to transplants. *Spine* 2001, 26, (24 Suppl), S13-22.
9. Oudega, M.; Gautier, S. E.; Chapon, P.; Frago, M.; Bates, M. L.; Parel, J. M.; Bunge, M. B., Axonal regeneration into Schwann cell grafts within resorbable poly(alpha-hydroxyacid) guidance channels in the adult rat spinal cord. *Biomaterials* 2001, 22, (10), 1125-36.
10. Takami, T.; Oudega, M.; Bates, M. L.; Wood, P. M.; Kleitman, N.; Bunge, M. B., Schwann cell but not olfactory ensheathing glia transplants improve hindlimb locomotor performance in the moderately contused adult rat thoracic spinal cord. *J Neurosci* 2002, 22, (15), 6670-81.

11. Filbin, M. T., Axon regeneration: Vaccinating against spinal cord injury. *Current Biology* 2000, *V10*, (N3), R100-R103.
12. Fournier, A. E.; Strittmatter, S. M., Repulsive factors and axon regeneration in the CNS. *Curr Opin Neurobiol* 2001, *11*, (1), 89-94.
13. Huber, A. B.; Weinmann, O.; Brosamle, C.; Oertle, T.; Schwab, M. E., Patterns of Nogo mRNA and protein expression in the developing and adult rat and after CNS lesions. *J Neurosci* 2002, *22*, (9), 3553-67.
14. Jones, L. L.; Tuszynski, M. H., Spinal cord injury elicits expression of keratan sulfate proteoglycans by macrophages, reactive microglia, and oligodendrocyte progenitors. *J Neurosci* 2002, *22*, (11), 4611-24.
15. Spencer, T.; Domeniconi, M.; Cao, Z.; Filbin, M. T., New roles for old proteins in adult CNS axonal regeneration. *Curr Opin Neurobiol* 2003, *13*, (1), 133-9.
16. Fallon, J. R., Preferential outgrowth of central nervous system neurites on astrocytes and Schwann cells as compared with nonglial cells in vitro. *J Cell Biol* 1985, *100*, (1), 198-207.
17. Gasser, U. E.; Hatten, M. E., Neuron-glia interactions of rat hippocampal cells in vitro: glial- guided neuronal migration and neuronal regulation of glial differentiation. *J Neurosci* 1990, *10*, (4), 1276-85.
18. Neugebauer, K. M.; Tomaselli, K. J.; Lilien, J.; Reichardt, L. F., N-cadherin, NCAM, and integrins promote retinal neurite outgrowth on astrocytes in vitro. *J Cell Biol* 1988, *107*, (3), 1177-87.
19. Noble, M.; Fok-Seang, J.; Cohen, J., Glia are a unique substrate for the in vitro growth of central nervous system neurons. *J Neurosci* 1984, *4*, (7), 1892-903.
20. Silver, J.; Lorenz, S. E.; Wahlsten, D.; Coughlin, J., Axonal guidance during development of the great cerebral commissures: descriptive and experimental studies, in vivo, on the role of preformed glial pathways. *J Comp Neurol* 1982, *210*, (1), 10-29.
21. Silver, J.; Robb, R. M., Studies on the development of the eye cup and optic nerve in normal mice and in mutants with congenital optic nerve aplasia. *Dev Biol* 1979, *68*, (1), 175-90.
22. Silver, J.; Rutishauser, U., Guidance of optic axons in vivo by a preformed adhesive pathway on neuroepithelial endfeet. *Dev Biol* 1984, *106*, (2), 485-99.

23. Silver, J.; Sidman, R. L., A mechanism for the guidance and topographic patterning of retinal ganglion cell axons. *J Comp Neurol* 1980, *189*, (1), 101-11.
24. Smith, G. M.; Miller, R. H.; Silver, J., Changing role of forebrain astrocytes during development, regenerative failure, and induced regeneration upon transplantation. *J Comp Neurol* 1986, *251*, (1), 23-43.
25. Liesi, P.; Dahl, D.; Vaehri, A., Laminin is produced by early rat astrocytes in primary culture. *J Cell Biol* 1983, *96*, (3), 920-4.
26. Liesi, P.; Kirkwood, T.; Vaehri, A., Fibronectin is expressed by astrocytes cultured from embryonic and early postnatal rat brain. *Exp Cell Res* 1986, *163*, (1), 175-85.
27. Liesi, P.; Silver, J., Is astrocyte laminin involved in axon guidance in the mammalian CNS? *Dev Biol* 1988, *130*, (2), 774-85.
28. Nathaniel, E.; Nathaniel, D., The reactive astrocyte. *Adv Cell Neurobiol* 1981, *2*, 249-301.
29. Selak, I.; Foidart, J. M.; Moonen, G., Laminin promotes cerebellar granule cells migration in vitro and is synthesized by cultured astrocytes. *Dev Neurosci* 1985, *7*, (5-6), 278-85.
30. Barrett, C. P.; Donati, E. J.; Guth, L., Differences between adult and neonatal rats in their astroglial response to spinal injury. *Exp Neurol* 1984, *84*, (2), 374-85.
31. Bignami, A.; Dahl, D., The astroglial response to stabbing: immunofluorescence studies with antibodies to astrocyte-specific protein (GFA) in mammalian and submammalian vertebrates. *Neuropathol Appl Neurobiol* 1976, *251*, 23-43.
32. Latov, N.; Nilaver, G.; Zimmerman, E. A.; Johnson, W. G.; Silverman, A. J.; Defendini, R.; Cote, L., Fibrillary astrocytes proliferate in response to brain injury: a study combining immunoperoxidase technique for glial fibrillary acidic protein and radioautography of tritiated thymidine. *Dev Biol* 1979, *72*, (2), 381-4.
33. Mathewson, A. J.; Berry, M., Observations on the astrocyte response to a cerebral stab wound in adult rats. *Brain Res* 1985, *327*, (1-2), 61-9.
34. McKeon, R. J.; Jurynek, M. J.; Buck, C. R., The chondroitin sulfate proteoglycans neurocan and phosphacan are expressed by reactive astrocytes in the chronic CNS glial scar. *J Neurosci* 1999, *19*, (24), 10778-88.

35. McKeon, R. J.; Schreiber, R. C.; Rudge, J. S.; Silver, J., Reduction of neurite outgrowth in a model of glial scarring following CNS injury is correlated with the expression of inhibitory molecules on reactive astrocytes. *J Neurosci* 1991, *11*, (11), 3398-411.
36. Reier, P.; Stensaas, L.; Guth, L., The astrocytic scar as an impediment to regeneration in the central nervous system. In *Spinal Cord Reconstruction*, Kao, C.; Bunge, R.; Reier, P., 'Eds.' Raven Press: New York, 1983; pp 163-195.
37. Smith, G. M.; Rutishauser, U.; Silver, J.; Miller, R. H., Maturation of astrocytes in vitro alters the extent and molecular basis of neurite outgrowth. *Dev Biol* 1990, *138*, (2), 377-90.
38. Davies, S. J.; Goucher, D. R.; Doller, C.; Silver, J., Robust regeneration of adult sensory axons in degenerating white matter of the adult rat spinal cord. *J Neurosci* 1999, *19*, (14), 5810-22.
39. Patist, C. M.; Mulder, M. B.; Gautier, S. E.; Maquet, V.; Jerome, R.; Oudega, M., Freeze-dried poly(D,L-lactic acid) macroporous guidance scaffolds impregnated with brain-derived neurotrophic factor in the transected adult rat thoracic spinal cord. *Biomaterials* 2004, *25*, (9), 1569-82.
40. Bomze, H. M.; Bulsara, K. R.; Iskandar, B. J.; Caroni, P.; Skene, J. H. P., Spinal axon regeneration evoked by replacing two growth cone proteins in adult neurons. *Nature Neuroscience* 2001, *4*, (N1), 38-43.
41. Lu, P.; Yang, H.; Jones, L. L.; Filbin, M. T.; Tuszynski, M. H., Combinatorial therapy with neurotrophins and cAMP promotes axonal regeneration beyond sites of spinal cord injury. *J Neurosci* 2004, *24*, (28), 6402-9.
42. McDonald, J. W.; Liu, X. Z.; Qu, Y.; Liu, S.; Mickey, S. K.; Turetsky, D.; Gottlieb, D. I.; Choi, D. W., Transplanted embryonic stem cells survive, differentiate and promote recovery in injured rat spinal cord. *Nat Med* 1999, *5*, (12), 1410-2.
43. Nikulina, E.; Tidwell, J. L.; Dai, H. N.; Bregman, B. S.; Filbin, M. T., The phosphodiesterase inhibitor rolipram delivered after a spinal cord lesion promotes axonal regeneration and functional recovery. *Proc Natl Acad Sci U S A* 2004, *101*, (23), 8786-90.
44. Pearse, D. D.; Pereira, F. C.; Marcillo, A. E.; Bates, M. L.; Berrocal, Y. A.; Filbin, M. T.; Bunge, M. B., cAMP and Schwann cells promote axonal growth and functional recovery after spinal cord injury. *Nat Med* 2004, *10*, (6), 610-6.

45. Steward, O.; Schauwecker, P. E.; Guth, L.; Zhang, Z.; Fujiki, M.; Inman, D.; Wrathall, J.; Kempermann, G.; Gage, F. H.; Saatman, K. E.; Raghupathi, R.; McIntosh, T., Genetic approaches to neurotrauma research: opportunities and potential pitfalls of murine models. *Experimental Neurology* 1999, *157*, (1), 19-42.
46. Woolf, C. J., Turbocharging neurons for growth: accelerating regeneration in the adult CNS. *Nature Neuroscience* 2001, *4*, (N1), 7-9.
47. Brodkey, J. A.; Gates, M. A.; Laywell, E. D.; Steindler, D. A., The complex nature of interactive neuroregeneration-related molecules. *Exp. Neurol.* 1993, *123*, 251-270.
48. Bronner Fraser, M.; Stern, C. D.; Fraser, S., Analysis of neural crest cell lineage and migration. *J. Craniofac. Genet. Dev. Biol.* 1991, *11*, 214-222.
49. Frisen, J., Determinants of axonal regeneration. *Histol. Histopathol* 1997, *12*, 857-868.
50. Luckenbill-Edds, L., Laminin and the mechanism of neuronal outgrowth. *Brain Res. Rev.* 1997, *23.1-2*, 1-27.
51. Uhm, J. H.; Gladson, C. L.; Rao, J. S., The role of integrins in the malignant phenotype of gliomas. *Front Biosci.* 1999, *15*, 1093-4715.
52. Zhang, Z.; Yoo, R. J.; Wells, M. C.; Beebe, J., Thomas P.; Biran, R.; Tresco, P., Neurite outgrowth on well-characterized surfaces: preparation and characterization of chemically and spatially controlled fibronectin and RGD substrates with good bioactivity. *Biomaterials* 2005, *26*, 47-61.
53. Bellamkonda, R.; Ranieri, J. P.; Aebischer, P., Laminin oligopeptide derivatized agarose gels allow three-dimensional neurite extension in vitro. *J. Neurosci. Res.* 1995, *41*, (4), 501-509.
54. Borkenhagen, M.; Clemence, J. F.; Sigrist, H.; Aebischer, P., Three-dimensional extracellular matrix engineering in the nervous system. *J. Biomed. Mater. Res.* 1998, *40*, (3), 392-400.
55. Clemence, J. F.; Ranieri, J. P.; Aebischer, P.; Sigrist, H., Photoimmobilization of a bioactive laminin fragment and pattern-guided selective neuronal cell attachment. *Bioconjug. Chem.* 1995, *6*, (4), 411-417.

56. Luckenbill-Edds, L.; Kaiser, C. A.; Rodgers, T. R.; Powell, D. D., Localization of the 110 kDa receptor for laminin in brains of embryonic and postnatal mice. *Cell Tissue Res.* 1995, 279, (2), 371-377.
57. Ranieri, J. P.; Bellamkonda, R.; Bekos, E. J.; Gardella, J. A. J.; Mathieu, H. J.; Ruiz, L.; Aebischer, P., Spatial control of neuronal cell attachment and differentiation on covalently patterned laminin oligopeptide substrates. *Int. J. Dev. Neurosci.* 1994, 12, (8), 725-735.
58. Ranieri, J. P.; Bellamkonda, R.; Bekos, E. J.; Vargo, T. G.; Gardella, J. A. J.; Aebischer, P., Neuronal cell attachment to fluorinated ethylene propylene films with covalently immobilized laminin oligopeptides YIGSR and IKVAV. II. *J. Biomed. Mater. Res.* 1995, 29, (6), 779-785.
59. Tashiro, K.; Sephel, G. C.; Weeks, B.; Sasaki, M.; Martin, G. R.; Kleinman, H. K.; Yamada, Y., A synthetic peptide containing the IKVAV sequence from the A chain of laminin mediates cell attachment, migration, and neurite outgrowth. *J. Biol. Chem.* 1989, 264, (27), 16174-16182.
60. Bhatia, S. K.; Shriver-Lake, L. C.; Prior, K. J.; Georger, J. H.; Calvert, J. M.; Bredehorst, R.; Ligler, F. S., Use of Thiol-Terminated Silanes and Heterobifunctional Crosslinkers for Immobilization of Antibodies on Silica Surfaces. *Analytical Biochemistry* 1989, 178, 408-413.
61. Neff, J. A.; Caldwell, K. D.; Tresco, P. A., A novel method for surface modification to promote cell attachment to hydrophobic substrates. *Journal of Biochemical Materials Research* 1997, 40, 511-519.
62. Liesi, P., Extracellular matrix and neuronal movement. *Experientia* 1990, 46, (9), 900-907.
63. Williams, J. M., Han, T., Beebe, T. P., Determination of single-bond forces from contact force variances in atomic force microscopy. *Langmuir* 1996, 12, (5), 1291-1295.
64. Lo, Y.-S.; Beebe, T. P., Jr., Loading-Rate Dependence of Individual Ligand-Receptor Bond-Rupture Forces Studied by Atomic Force Microscopy. *Langmuir* 2001, 17, (12), 3741-3748.
65. Lo, Y.-S.; Huefner, N. D.; Chan, W. S.; Stevens, F.; Harris, J. M.; Beebe, T. P., Jr., Specific interactions between biotin and avidin studied by atomic force microscopy using the Poisson statistical analysis method. *Langmuir* 1999, 15, (4), 1373-1382.

66. Lo, Y.-S.; Simons, J.; Beebe, T. P., Jr., Temperature Dependence of the Biotin-Avidin Bond-Rupture Force Studied by Atomic Force Microscopy. *Journal of Physical Chemistry B* 2002, *106*, (38), 9847-9852.
67. Bognitzki, M.; Frese, T.; Wendorff, J. H.; Greiner, A., Submicrometer shaped polylactide fibers by electrospinning. *Polymeric Materials Science and Engineering* 2000, *82*, 115-116.
68. Casper, C. L.; Stephens, J. S.; Tassi, N. G.; Chase, D. B.; Rabolt, J. F., Controlling Surface Morphology of Electrospun Polystyrene Fibers: Effect of Humidity and Molecular Weight in the Electrospinning Process. *Macromolecules* 2004, *37*, (2), 573-578.
69. Doshi, J.; Reneker, D. H., Electrospinning process and applications of electrospun fibers. *Journal of Electrostatics* 1995, *35*, (2&3), 151-60.
70. Fong, H.; Chun, I.; Reneker, D. H., Beaded nanofibers formed during electrospinning. *Polymer* 1999, *40*, (16), 4585-4592.
71. Huang, Z.-M.; Zhang, Y. Z.; Kotaki, M.; Ramakrishna, S., A review on polymer nanofibers by electrospinning and their applications in nanocomposites. *Composites Science and Technology* 2003, *63*, (15), 2223-2253.
72. Jaeger, R.; Bergshoef, M. M.; Martin i Batlle, C.; Schoenherr, H.; Vancso, G. J., Electrospinning of ultrathin polymer fibers. *Macromolecular Symposia* 1998, *127*, (Rolduc Polymer Meeting 10: \"Petro\" Polymers vs. \"Green\" Polymers, 1997), 141-150.
73. Koombhongse, S.; Liu, W.; Reneker, D. H., Flat polymer ribbons and other shapes by electrospinning. *Journal of Polymer Science, Part B: Polymer Physics* 2001, *39*, (21), 2598-2606.
74. Matthews, J. A.; Wnek, G. E.; Simpson, D. G.; Bowlin, G. L., Electrospinning of Collagen Nanofibers. *Biomacromolecules* 2002, *3*, (2), 232-238.
75. Megelski, S.; Stephens, J. S.; Chase, D. B.; Rabolt, J. F., Micro- and nanostructure surface morphology on electrospun polymer fibers. *Macromolecules* 2002, *35*, (22), 8456-8466.
76. Reneker, D. H.; Chun, I., Nanometer diameter fibers of polymer, produced by electrospinning. *Nanotechnology* 1996, *7*, (3), 216-223.
77. Srinivasan, G.; Reneker, D. H., Structure and morphology of small diameter electrospun aramid fibers. *Polymer International* 1995, *36*, (2), 195-201.

78. Matthews, J. A.; Boland, E. D.; Wnek, G. E.; Simpson, D. G.; Bowlin, G. L., Electrospinning of collagen type II: a feasibility study. *Journal of Bioactive and Compatible Polymers* 2003, 18, (2), 125-134.
79. McNally, H. A., Borgens, Richard Ben, Three-dimensional imaging of living and dying neurons with atomic force microscopy. *Journal of Neurocytology* 2004, 33, 251-258.
80. Palecek, S. P.; Loftus, J. C.; Ginsberg, M. H.; Lauffenburger, D. A.; Horwitz, A. F., Integrin-ligand binding properties govern cell migration speed through cell-substratum adhesiveness. *Nature* 1997, 385, (6616), 537-40.
81. Condic, M. L.; Letourneau, P. C., Ligand-induced changes in integrin expression regulate neuronal adhesion and neurite outgrowth. *Nature* 1997, 389, (6653), 852-6.
82. Adamson, A. W.; Gast, A. P., *Physical Chemistry of Surfaces*. 6 ed.; John Wiley & Sons, Inc.: New York, 1997.
83. Benninghoven, A., Surface investigation of solids by the statistical method of secondary ion mass spectrometry (SIMS). *Surface Science* 1973, 35, 427-457.
84. Niehuis, E.; Heller, T.; Feld, H.; Benninghoven, A., Design and performance of a reflectron based time-of-flight secondary ion mass spectrometer with electrodynamic primary ion mass separation. *Journal of Vacuum Science and Technology* 1987, 5, 1243-1246.
85. Canavan, H. E.; Cheng, X.; Graham, D. J.; Ratner, B. D.; Castner, D. G., Surface Characterization of the Extracellular Matrix Remaining after Cell Detachment from a Thermoresponsive Polymer. *Langmuir* 2005, 21, (5), 1949-1955.
86. Hyun, J.; Ma, H.; Zhang, Z.; Beebe, J., Thomas P., Universal route to cell micropatterning using an amphiphilic comb polymer. *Advanced Materials* 2003, 15, (7-8), 576-579.
87. Kingshott, P.; McArthur, S.; Thissen, H.; Castner, D. G.; Griesser, H. J., Ultrasensitive probing of the protein resistance of PEG surfaces by secondary ion mass spectrometry. *Biomaterials* 2002, 23, (24), 4775-4785.
88. Lhoest, J. B.; Wagner, M. S.; Tidwell, C. D.; Castner, D. G., Characterization of adsorbed protein films by time of flight secondary ion mass spectrometry. *Journal of Biomedical Materials Research* 2001, 57, (3), 432-440.

89. Tidwell, C. D.; Castner, D. G.; Golledge, S. L.; Ratner, B. D.; Meyer, K.; Hagenhoff, B.; Benninghoven, A., Static time-of-flight secondary ion mass spectrometry and x-ray photoelectron spectroscopy characterization of adsorbed albumin and fibronectin films. *Surface and Interface Analysis* 2001, *31*, (8), 724-733.
90. Belu, A. M.; Graham, D. J.; Castner, D. G., Time-of-flight secondary ion mass spectrometry: techniques and applications for the characterization of biomaterial surfaces. *Biomaterials* 2003, *24*, 3635-3653.
91. Chu, P. K.; Odom, R. W.; Reich, D. F., Analysis of surface particles by time-of-flight secondary ion mass spectrometry. *Materials Chemistry and Physics* 1996, *43*, (2), 87-94.
92. Léonard, D.; Mathieu, H. J., *Fresenius Journal of Analytical Chemistry*. 365 1999, (3-11).
93. Bi, J.; Downs, J. C.; Jacob, J. T., Tethered protein/peptide-surface-modified hydrogels. *Journal of Biomaterials Science* 2004, *15*, (7), 905-916.
94. Lom, B.; Healy, K. E.; Hockberger, P. E., A versatile technique for patterning biomolecules onto glass coverslips. *Journal of Neuroscience Methods* 1993, *50*, (3), 385-397.
95. Matsuzawa, M.; Umemura, K.; Beyer, D.; Sugioka, K.; Knoll, W., Micropatterning of neurons using organic substrates in culture. *Thin Solid Films* 1997, *305*, (1,2), 74-79.
96. Ruiz, L.; Fine, E.; Voros, J.; Makohliso, S. A.; Leonard, D.; Johnston, D. S.; Textor, M.; Mathieu, H. J., Phosphorylcholine-containing polyurethanes for the control of protein adsorption and cell attachment via photoimmobilized laminin oligopeptides. *Journal of Biomaterials Science* 1999, *10*, (9), 931-955.
97. Saneinejad, S.; Shoichet, M. S., Patterned glass surfaces direct cell adhesion and process outgrowth of primary neurons of the central nervous system. *Journal of Biomedical Materials Research* 1998, *42*, 13-19.
98. Hayakawa, T.; Yoshinari, M.; Nagai, M.; Yamamoto, M.; Nemoto, K., X-ray photoelectron spectroscopic studies of the reactivity of basic terminal OH of titanium towards tresyl chloride and fibronectin. *Biomedical Research* 2003, *24*, (5), 223-230.

99. Smith, J. T.; Tomfohr, J. K.; Wells, M. C.; Beebe, J., Thomas P.; Kepler, T. B.; Reichert, W. M., Measurement of Cell Migration on Surface-Bound Fibronectin Gradients. *Langmuir* 2004, 20, 8279-8286.
100. O'Connor, D. J.; Sexton, B. A.; Smart, S. C., *Surface analysis method in materials science*. Springer-Verlag: Heidelberg, 1992.
101. Johnson, W. C.; Stein, D. F.; Joshi, A., Auger electron spectroscopy. Review. *Canadian Journal of Spectroscopy* 1972, 17, (3), 88-92.
102. Turner, N. H., Auger electron spectroscopy. In *Handbook of Surface Imaging and Visualization*, Hubbard, A. T., 'Ed.'; CRC Press: Boca Raton, 1995; pp 33-43.
103. Turner, N. H.; Dunlap, B. I.; Colton, R. J., Surface analysis: x-ray photoelectron spectroscopy, Auger electron spectroscopy and secondary ion mass spectrometry. *Analytical Chemistry* 1984, 56, (5), 373R-416R.
104. Cumpson, P. J., Angle-resolved XPS and AES: depth-resolution limits and a general comparison of properties of depth-profile reconstruction methods. *Journal of Electron Spectroscopy and Related Phenomena* 1995, 73, (1), 25-52.
105. Diao, J.; Hess, D. W., Use of angle-resolved XPS to determine depth profiles based on Fick's second law of diffusion: description of method and simulation study. *Journal of Electron Spectroscopy and Related Phenomena* 2004, 135, (2-3), 87-104.
106. Hollander, J. M.; Jolly, W. L., X-ray Photoelectron Spectroscopy. *Accounts of Chemical Research* 1970, 3, (6), 193-200.
107. Xia, Y.; Whitesides, G. M., Soft Lithography. *Angewandte Chemie International Edition* 1998, 37, 550-575.
108. Kumar, A.; Biebuyck, H.; Whitesides, G. M., Patterning Self-Assembled Monolayers: Applications in Materials Science. *Langmuir* 1994, 10, (5), 1498-1511.
109. Amirpour, M. L. G., Pradyut; Lackowski, William M.; Crooks, Richard M.; Pishko, Michael V., Mammalian cell cultures on micropatterned surfaces of weak-acid, polyelectrolyte hyperbranched thin films on gold. *Analytical Chemistry* 2001, 73, (7), 1560-1566.

110. Craighead, H. G. T., S. W.; Davis, R. C.; James, C.; Perez, A. M.; St. John, P. M.; Isaacson, M. S.; Kam, L.; Shain, W.; Turner, J. N.; Banker, G., Chemical and topographical surface modification for control of central nervous system cell adhesion. *Biomedical Microdevices* 1998, 1, (1), 49-64.
111. Lu, L. K., Lance; Hasenbein, Meredith; Nyalakonda, Kavita; Bizios, Rena; Gopferich, Achim; Young, James F.; Mikos, Antonios G., Retinal pigment epithelial cell function on substrates with chemically micropatterned surfaces. *Biomaterials* 1999, 20, (23-24), 2351-2361.
112. Mrksich, M. C., Christopher S.; Xia, Younan; Dike, Laura E.; Ingber, Donald E.; Whitesides, George M., Controlling cell attachment on contoured surfaces with self-assembled monolayers of alkanethiolates on gold. *Proceedings of the National Academy of Sciences of the United States of America* 1996, 93, (20), 10775-10778.
113. Mrksich, M. D., L E; Tien, J; Ingber, D E; Whitesides, G M, Using microcontact printing to pattern the attachment of mammalian cells to self-assembled monolayers of alkanethiolates on transparent films of gold and silver. *Experimental Cell Research* 1997, 235, (2), 305-13.
114. Zhang, S. Y., Lin; Altman, Michael; Lasse, Michael; Nugent, Helen; Frankel, Felice; Lauffenburger, Douglas A.; Whitesides, George M.; Rich, Alexander., Biological surface engineering: a simple system for cell pattern formation. *Biomaterials* 1999, 20, (13), 1213-1220.
115. Bernard, A.; Delamarche, E.; Schmid, H.; Michel, B.; Bosshard, H. R.; Biebuyck, H., Printing Patterns of Proteins. *Langmuir* 1998, 14, (9), 2225-2229.
116. Bernard, A.; Renault, J. P.; Michel, B.; Bosshard, H. R.; Delamarche, E., Microcontact Printing of Proteins. *Advanced Materials* 2000, 12, (14), 1067-1070.
117. Inerowicz, H. D.; Howell, S.; Regnier, F. E.; Reifenger, R., Multiprotein Immunoassay Arrays Fabricated by Microcontact Printing. *Langmuir* 2002, 18, 5263-5268.
118. Tan, J. L.; Tien, J.; Chen, C. S., Microcontact Printing of Proteins on Mixed Self-Assembled Monolayers. *Langmuir* 2002, 18, 519-523.
119. Desai, N. P.; Hubbell, J. A., Surface modifications of polymeric biomaterials for reduced thrombogenicity. *Polymeric Materials Science and Engineering* 1990, 62, 731-735.

120. Gombotz, W. R.; Guanghai, W.; Horbett, T. A.; Hoffman, A. S., Protein adsorption to poly(ethylene oxide) Surfaces. *Journal of Biomedical Materials Research* 1991, 25, 1547-1562.
121. Grasel, T. G.; Cooper, S. L., Surface properties and blood compatibility of polyurethanes. *Biomaterials* 1986, 7, 315-328.
122. Lee, J. H.; Kopecek, J.; Andrade, J., Surface properties of aqueous PEO-containing block copolymer surfactants: Protein resistant surfaces. *Polymeric Materials Science and Engineering* 1987, 57, 613-617.
123. Wasiewski, W.; Fasco, M. J.; Martin, B. M.; Detwiler, T. C.; Fenton, J. W., Thrombin adsorption to surfaces and prevention with polyethylene glycol 6000. *Thrombosis Research* 1976, 8, 881-886.
124. Desai, N. P.; Hubbell, J. A., Biological responses to polyethylene oxide modified polyethylene terephthalate surfaces. *Journal of Biomedical Materials Research* 1991, 25, 829-843.
125. Grainger, D. W.; Nojiri, C.; Okano, T.; Kim, S. W., In vitro and ex vitro platelet interactions with hydrophilic-hydrophobic poly(ethylene oxide)-heparin block copolymers. I. Synthesis and characterization. *Journal of Biomedical Materials Research* 1988, 22, 231-249.
126. Shoichet, M. S.; Winn, S. R.; Athavale, S.; Harris, J. M.; Gentile, F. T., Poly(ethylene oxide)-grafted thermoplastic membranes for use as cellular hybrid bio-artificial organs in the central nervous system. *Biotechnology and Bioengineering* 1994, 43, 563-572.
127. Zhang, Z.; Hyun, J.; Ma, H.; Chilkoti, A.; Beebe, J., Thomas P., Reorientation of Comb Polymer Surfaces Affects Protein Adsorption. *Langmuir* submitted.
128. Irvine, D. J. M., Anne M.; Griffith, Linda G., Nanoscale Clustering of RGD Peptides at Surfaces Using Comb Polymers. 1. Synthesis and Characterization of Comb Thin Films. *Biomacromolecules* 2001, 2, (1), 85-94.
129. Ma, H.; Hyun, J.; Zhang, Z.; Beebe, J., Thomas P.; Chilkoti, A., Fabrication of Biofunctionalized Quasi-Three-Dimensional Microstructures of a Nonfouling Comb Polymer Using Soft Lithography. *Advanced Functional Materials* 2005, 15, (4), 529-540.
130. Egolf-Fox, H. S.; Boggs, M. E.; Yoo, R. J.; Zhang, Z.; Beebe, J., Thomas P., Reproducibility in Comb Polymer Micro-contact Printing for Neuronal Guidance. *Biomacromolecules* submitted.

131. Cajal, S. R. Y., *Degeneration and Regeneration of the Nervous System* (trans. May R. M.). Oxford University Press: London, 1928.
132. Goodman, C. S., Mechanisms and molecules that control growth cone guidance. *Annual Review of Neuroscience* 1996, 19, 341-377.
133. Lauffenburger, D. A.; Horwitz, A. F., Cell Migration: A Physically Integrated Molecular Process. *Cell* 1996, 84, 359-369.
134. Mueller, B. K., Growth cone guidance: first steps towards a deeper understanding. *Annual Review of Neuroscience* 1999, 22, 351-388.
135. Parent, C. A.; Devreotes, P. N., A Cell's Sense of Direction. *Science* 1999, 284, 765-770.
136. Paves, H.; Saarma, M., Neurotrophins as in vitro growth cone guidance molecules for embryonic sensory neurons. *Cell and Tissue Research* 1997, 290, (2), 285-297.
137. Zheng, J. Q.; Wan, J.-j.; Poo, M.-m., Essential Role of Filopodia in Chemotropic Turning of Nerve Growth Cone Induced by a Glutamate Gradient. *Journal of Neuroscience* 1996, 16, (3), 1140-1149.
138. Caelen, I.; Bernard, A.; Juncker, D.; Michel, B.; Heinzelmann, H.; Delamarche, E., Formation of Gradients of Proteins on Surfaces with Microfluidic Networks. *Langmuir* 2000, 16, 9125-9130.
139. Caterina, M. J.; Devreotes, P. N., Molecular insights into eukaryotic chemotaxis. *Federation of American Societies for Experimental Biology* 1991, 5, (15), 3078-3085.
140. Cheng, H.-J.; Nakamoto, M.; Bergemann, A. D.; Flanagan, J. G., Complementary Gradients in Expression and Binding of ELF-1 and Mek4 in Development of the Topographic Retinotectal Projection Map. *Cell* 1995, 82, 371-381.
141. Devreotes, P. N.; Zigmond, S. H., Chemotaxis in eukaryotic cells: a focus on leukocytes and Dictyostelium. *Annual Review of Cell Biology* 1988, 4, 649-686.
142. Feldheim, D. A.; Vanderhaeghen, P.; Hansen, M. J.; Frisén, J.; Lu, Q.; Barbacid, M.; Flanagan, J. G., Topographic Guidance Labels in a Sensory Projection to the Forebrain. *Neuron* 1998, 21, 1303-1313.

143. Gundersen, R. W.; Barrett, J. N., Neuronal chemotaxis: chick dorsal-root axons turn toward high concentrations of nerve growth factor. *Science* 1979, 206, (4422), 1079-1080.
144. Gundersen, R. W.; Barrett, J. N., Characterization of the turning response of dorsal root neurites toward nerve growth factor. *Journal of Cell Biology* 1980, 87, (3 Pt 1), 546-554.
145. Keynes, R.; Cook, G. M. W., Axon Guidance Molecules. *Cell* 1995, 83, 161-169.
146. Keynes, R.; Tannahill, D.; Morgenstern, D. A.; Johnson, A. R.; Cook, G. M. W.; Pini, A., Surround Repulsion of Spinal Sensory Axons in Higher Vertebrate Embryos. *Neuron* 1997, 18, 889-897.
147. Knapp, D. M.; Helou, E. F.; Tranquillo, R. T., A Fibrin or Collagen Gel Assay for Tissue Cell Chemotaxis: Assessment of Fibroblast Chemotaxis to GRGDSP. *Experimental Cell Research* 1999, 247, 543-553.
148. Mato, J. M.; Losada, A.; Nanjundiah, V.; Konjin, T. M., Signal input for a chemotactic response in the cellular slime mold *Dictyostelium discoideum*. *Proceedings of the National Academy of Sciences of the United States of America* 1975, 72, (12), 4991-4993.
149. Tessier-Lavigne, M.; Goodman, C. S., The Molecular Biology of Axon Guidance. *Science* 1996, 274, (5290), 1123-1133.
150. Tessier-Lavigne, M.; Placzek, M.; Lumsden, A. G.; Dodd, J.; Jessell, T. M., Chemotropic guidance of developing axons in the mammalian central nervous system. *Nature* 1988, 336, (6201), 775-778.
151. Zigmond, S. H., Consequences of chemotactic peptide receptor modulation for leukocyte orientation. *Journal of Cell Biology* 1981, 88, (3), 644-647.
152. Baier, H.; Bonhoeffer, F., Axon guidance by gradients of a target-derived component. *Science* 1992, 255, (5043), 472-475.
153. Halfter, W., The Behavior of Optic Axons on Substrate Gradients of Reintal Basal Lamina Proteins and Merosin. *Journal of Neuroscience* 1996, 16, (14), 4389-4401.
154. Kapur, T. A.; Shoichet, M. S., Immobilized concentration gradients of nerve growth factor guide neurite outgrowth. *Journal of Biomedical Materials Research* 2004, 68A, 235-243.

155. Pérez, N. L.; Sosa, M. A.; Kuffler, D. P., Growth Cones Turn up Concentration Gradients of Diffusible Peripheral Target-Derived Factors. *Experimental Neurology* 1997, *145*, 196-202.
156. Song, H.-j.; Ming, G.-l.; Poo, M.-m., cAMP-induced switching in turning direction of nerve growth cones. *Nature* 1997, *388*, 275-279.
157. Stokes, C. L.; Rupnick, M. A.; Williams, S. K.; Lauffenburger, D. A., Chemotaxis of human microvessel endothelial cells in response to acidic fibroblast growth factor. *Laboratory Investigation* 1990, *63*, (5), 657-668.
158. Zheng, M.; Kuffler, D. P., Guidance of Regenerating Motor Axons *In Vivo* by Gradients of Diffusible Peripheral Nerve-Derived Factors. *Journal of Neurobiology* 2000, *42*, 212-219.
159. Carter, S. B., Principles of cell motility: the direction of cell movement and cancer invasion. *Nature* 1965, *208*, (16), 1183-1187.
160. Adams, D. N.; Kao, E., Y. C.; Hypolite, C. L.; Distefano, M. D.; Hu, W.-S.; Letourneau, P. C., Growth Cones Turn and Migrate up an Immobilized Gradient of the Laminin IKVAV Peptide. *Journal of Neurobiology* 2005, *62*, 134-147.
161. Cao, X.; Shoichet, M. S., Defining the Concentration Gradient of Nerve Growth Factor for Guided Neurite Outgrowth. *Neuroscience* 2001, *103*, (3), 831-840.
162. Goodhill, G. J., Diffusion in axon guidance. *European Journal of Neuroscience* 1997, *9*, (7), 1414-1421.
163. Matsuzawa, M.; Tokumitsu, S.; Knoll, W.; Liesi, P., Molecular Gradient Along the Axon Pathway Is Not Required for Directional Axon Growth. *Journal of Neuroscience Research* 1998, *53*, 114-124.
164. Daniel, S.; Chaudhury, M. K., Rectified Motion of Liquid Drops on Gradient Surfaces Induced by Vibration. *Langmuir* 2002, *18*, 3404-3407.
165. Daniel, S.; Chaudhury, M. K.; Chen, J. C., Fast Drop Movements Resulting from the Phase Change on a Gradient Surface. *Science* 2001, *291*, 633-636.
166. Ruardy, T. G.; Moorlag, H. E.; Schakenraad, J. M.; van der Mei, H. C.; Busscher, H. J., Growth of Fibroblasts and Endothelial Cells on Wettability Gradient Surfaces. *Journal of Colloid and Interface Science* 1997, *188*, 209-217.

167. Zhao, H.; Beysens, D., From Droplet Growth to Film Growth on a Heterogeneous Surface: Condensation Associated with a Wettability Gradient. *Langmuir* 1995, *11*, 627-634.
168. Delamarche, E.; Bernard, A.; Schmid, H.; Michel, B.; Biebuyck, H., Patterned Delivery of Immunoglobulins to Surfaces Using Microfluidic Networks. *Science* 1997, *276*, 779-781.
169. Dertinger, S. K.; Chiu, D. T.; Jeon, N. L.; Whitesides, G. M., Generation of Gradients Having Complex Shapes Using Microfluidic Networks. *Analytical Chemistry* 2001, *73*, 1240-1246.
170. Fosser, K. A.; Nuzzo, R. G., Fabrication of Patterned Multicomponent Protein Gradients and Gradient Arrays Using Microfluidic Depletion. *Analytical Chemistry* 2003, *75*, (21), 5775-5782.
171. Jeon, N. L.; Dertinger, S. K.; Chiu, D. T.; Choi, I. S.; Stroock, A. D.; Whitesides, G. M., Generation of Solution and Surface Gradients Using Microfluidic Systems. *Langmuir* 2000, *16*, 8311-8316.
172. Lohoff, A. M.; Quillan, M.; Dan, Y.; Poo, M.-m., Asymmetric modulation of cytosolic cAMP activity induces growth cone turning. *Journal of Neuroscience* 1992, *12*, (4), 1253-1261.
173. Zheng, J. Q.; Felder, M.; Connor, J. A.; Poo, M.-m., Turning of nerve growth cones induced by neurotransmitters. *Nature* 1994, *368*, (6467), 140-144.
174. Ruardy, T. G.; Schakenraad, J. M.; van der Mei, H. C.; Busscher, H. J., Adhesion and spreading of human skin fibroblasts on physicochemically characterized gradient surfaces. *Journal of Biomedical Materials Research* 1995, *29*, (11), 1415-1423.
175. Grabar, K. C.; Allison, K. J.; Baker, B. E.; Bright, R. M.; Brown, K. R.; Freeman, R. G.; Fox, A. P.; Keating, C. D.; Musick, M. D.; Natan, M. J., Two-Dimensional Arrays of Colloidal Gold Particles: A Flexible Approach to Macroscopic Metal Surfaces. 1996.
176. Lestelius, M.; Engquist, I.; Tengvall, P.; Chaudhury, M. K.; Liedberg, B., Order/disorder gradients of *n*-alkanethiols on gold. *Colloids and Surfaces B: Biointerfaces* 1999, *15*, 57-70.
177. Liedberg, B.; Tengvall, P., Molecular Gradients of  $\alpha$ -Substituted Alkanethiols on Gold Studied by X-ray Photoelectron Spectroscopy. *Langmuir* 1995, *11*, 3821-3827.

178. Liedberg, B.; Wirde, M.; Tao, Y.-T.; Tengvall, P.; Gelius, U., Molecular Gradients of  $\omega$ -Substituted Alkanethiols on Gold Studied by X-ray Photoelectron Spectroscopy. *Langmuir* 1997, *13*, 5329-5334.
179. Morgenthaler, S.; Lee, S.; Zürcher, S.; Spencer, N. D., A Simple, Reproducible Approach to the Preparation of Surface-Chemical Gradients. *Langmuir* 2003, *19*, (25), 10459-10462.
180. Welin-Klintström, S.; Lestelius, M.; Liedberg, B.; Tengvall, P., Comparison between wettability gradients made on gold and on Si/SiO<sub>2</sub> substrates. *Colloids and Surfaces B: Biointerfaces* 1999, *15*, 81-87.
181. Lee, J. H.; Kim, H. G.; Khang, G. S.; Lee, H. B.; Jhon, M. S., Characterization of wettability gradient surfaces prepared by corona discharge treatment. *Journal of Colloid and Interface Science* 1992, *151*, (2), 563-570.
182. Lee, J. H.; Lee, H. B., Platelet adhesion onto wettability gradient surfaces in the absence and presence of plasma proteins. *Journal of Biomedical Materials Research* 1998, *41*, 304-311.
183. Krauss, A. H. P.; Nieves, A. L.; Spada, C. S.; Woodward, D. F., Determination of leukotriene effects on human neutrophil chemotaxis in vitro by differential assessment of cell motility and polarity. *Journal of Leukocyte Biology* 1994, *55*, (2), 201-208.
184. Nagahata, H.; Nochi, H.; Tamoto, K.; Yamashita, K.; Noda, H.; Kociba, G. J., Characterization of functions of neutrophils from bone marrow of cattle with leukocyte adhesion deficiency. *American Journal of Veterinary Research* 1995, *56*, (2), 167-171.
185. Nelson, R. D.; Ouie, P. G.; Simmons, R. L., Chemotaxis under agarose: a new and simple method for measuring chemotaxis and spontaneous migration of human polymorphonuclear leukocytes and monocytes. *Journal of Immunology* 1975, *115*, (6), 1650-1656.
186. Plummer, S. T.; Wang, Q.; Bohn, P. W., Electrochemically Derived Gradients of the Extracellular Matrix Protein Fibronectin on Gold. *Langmuir* 2003, *19*, 7528-7536.
187. Terrill, R. H.; Balss, K. M.; Zhang, Y.; Bohn, P. W., Dynamic Monolayer Gradients: Active Spatiotemporal Control of Alkanethiol Coatings on Thin Gold Films. *Journal of the American Chemical Society* 2000, *122*, 988-989.

188. Wang, Q.; Bohn, P. W., Active Spatiotemporal Control of Arg-Gly-Asp-Containing Tetradecapeptide Organomercaptans on Gold with In-Plane Electrochemical Potential Gradients. *Journal of Physical Chemistry B* 2003, *107*, 12578-12584.
189. Caelen, I.; Gao, H.; Sigrist, H., Protein Density Gradients on Surfaces. *Langmuir* 2002, *18*, 2463-2467.
190. Efimenko, K.; Genzer, J., How to Prepare Tunable Planar Molecular Chemical Gradients. *Advanced Materials* 2001, *13*, (20), 1560-1563.
191. Genzer, J.; Fischer, D. A.; Efimenko, K., Fabricating Two-Dimensional Molecular Gradients via Asymmetric Deformation of Uniformly-Coated Elastomer Sheets. *Advanced Materials* 2003, *15*, (18), 1545-1547.
192. Hypolite, C. L.; McLernon, T. L.; Adams, D. N.; Chapman, K. E.; Herbert, C. B.; Huang, C. C.; Distefano, M. D.; Hu, W.-S., Formation of Microscale Gradients of Protein Using Heterobifunctional Photolinkers. *Bioconjugate Chemistry* 1997, *8*, 658-663.
193. Krämer, S.; Xie, H.; Gaff, J.; Williamson, J. R.; Tkachenko, A. G.; Nouri, N.; Feldheim, D. A.; Feldheim, D. L., Preparation of Protein Gradients through the Controlled Deposition of Protein-Nanoparticle Conjugates onto Functionalized Surfaces. *Journal of the American Chemical Society* 2004, *126*, 5388-5395.
194. Ruardy, T. G.; Schakenraad, J. M.; van der Mei, H. C.; Busscher, H. J., Preparation and characterization of chemical gradient surfaces and their application for the study of cellular interaction phenomena. *Surface Science Reports* 1997, *29*, 1-30.
195. Tomlinson, M. R.; Genzer, J., Formation of surface-grated copolymer brushes with continuous composition gradients. *Chemical Communications* 2003, 1350-1351.
196. Tomlinson, M. R.; Genzer, J., Formation of Grafted Macromolecular Assemblies with a Gradual Variation of Molecular Weight on Solid Substrates. *Macromolecules* 2003, *36*, (10), 3450-3451.
197. Tong, Y. W.; Shoichet, M. S., Enhancing the neuronal interaction on fluoropolymer surfaces with mixed peptides or spacer group linkers. *Biomaterials* 2001, *22*, 1029-1034.

198. Wu, T.; Efimenko, K.; Vlček, P.; Šubr, V.; Genzer, J., Formation and Properties of Anchored Polymers with a Gradual Variation of Grafting Densities on Flat Substrates. *Macromolecules* 2003, *36*, 2448-2453.